Abstract

Spatially localized structures are key components of turbulence and other spatio-temporally chaotic systems. From a dynamical systems viewpoint, it is desirable to obtain corresponding exact solutions, though their existence is not guaranteed. A damping filter method is introduced to obtain variously localized solutions, and adopted into two typical cases. This method introduces a spatially selective damping effect to make a good guess at the exact solution, and we can obtain an exact solution through a continuation with the damping amplitude. First target is a steady solution to Swift-Hohenberg equation, which is a representative of bi-stable systems in which localized solutions coexist, and a model for span-wisely localized cases. Not only solutions belonging to the well-known snaking branches but also those belonging to an isolated branch known as "isolas" are found with a continuation path between them in phase space extended with the damping amplitude. This indicates that this spatially selective excitation mechanism has an advantage in searching spatially localized solutions. Second target is a spatially localized traveling-wave solution to Kuramoto-Sivashinsky equation, which is a model for stream-wisely localized cases. Since the spatially selective damping effect breaks Galilean and translational invariances, the propagation velocity cannot be determined uniquely while the damping is active, and a singularity arises when these invariances are recovered. We demonstrate that this singularity can be avoided by imposing a simple condition, and a localized traveling-wave solution is obtained with a specific propagation speed.

An interface structure between turbulence and laminar flow is investigated in two-dimensional channel flow. This spatially localized structure not only sustains itself, but also converts laminar state into turbulence actively. A filtered simulation technique is introduced to understand the invading process as an inhomogeneity-induced self-sustaining coherent structure, which consists of a meandering jet on bulk region and near wall vortex pairs. A phenomenological model, called ejection-jet cycle, reveals the relationship between the spatial structure of the fat interface and its invading speed. This model gives a novel insight on the inner-outer interaction in wall-turbulence.

Spatially localized self-sustaining mechanism induced by inhomogeneity in turbulence

Toshiki Teramura

Division of Physics and Astronomy,
Graduate School of Science, Kyoto University, Japan

Ph.D. thesis submitted on January 7, 2016

Acknowledgements

First of all, I would like to express my special appreciation and thanks to my advisor Professor Dr. Sadayoshi Toh, you have been a tremendous mentor for me. I would like to thank you for encouraging my research and for allowing me to grow as a research scientist.

I am grateful to Dr. Takeshi Matsumoto, your invaluable advice and suggestions on my research and college life were enormous help to me. I also would like to thank my friends in my Fluid Physics Group, Atsushi Mizuta, Shunsuke Kohno, Yusuke Okahashi, Kentaro Takagi, Naoya Matsubara, Tomohiro Kosaka, Shunsuke Akita, Naohiro Temmoku, Yoshiki Hiruta, Ryo Murakami, Tin Unkai, and friends in Nonlinear Dynamics Group, Takahiro Nemoto, and Daisuke Sato for their discussion, comments, and suggestions.

I would like to thank all staffs in Kyoto University. My research is supported by the Grant-in-Aid for JSPS Fellows No.26·1005 and the Grants for Excellent Graduate Schools "The Next Generation of Physics, Spun from Universality and Emergence" from the Ministry of Education, Culture, Sports, Science, and Technology (MEXT) of Japan, and also partially by JSPS KAKENHI Grant Number 22540386. A part of numerical calculations were carried out on SR16000 at YITP in Kyoto University.

Finally, I would like to express a special thanks to my family for constant encouragement and tireless support.

Contents

Chapter 1

General Introduction

1.1 Inhomogeneous dynamics in nature

Inhomogeneous states appear in various types of uniform systems: spatial patterns in chemical reactions [18], localized turbulence in various canonical flows [1, 2], and chimera states in coupled oscillators [20]. Classical weakly nonlinear theories have revealed a class of pattern formulations, but most dynamic inhomogeneous states cannot be included in this class. These strongly nonlinear regimes have been investigated with computer simulations and it has been clarified that inhomogeneous states have much richer dynamics than uniform states since the inhomogeneity itself works as a component of the dynamics. Therefore, comprehensive theories for understanding of these dynamic self-organization are required for prediction and control in weather forecast, robotics, and life science. While many recent studies about inhomogeneity induced dynamics are devoted to discrete systems like coupled oscillators [45], in this thesis we consider a continuous system, namely turbulence .

Turbulence ubiquitously appears in nature: from quark-gluon plasma [53] to the Universe [15]. Because of its strong nonlinearity, most studies related to turbulence may have adopted more or less statistical or coarse graining approaches [10]. Though they have vividly revealed phenomenological and/or kinematic natures of turbulence such as the energy transfer among different scales and places, these statistical treatments are not sufficiently adequate to elucidate concrete mechanisms of even such fundamental processes of turbulence: For example, what substance, e.g. vortices, transfers energy or why the energy transfer occurs. On the other hand, the dynamical systems approaches to turbulence have helped us describe these mechanisms with numerically obtained components (invariant sets) in the phase space such as fixed points, periodic orbits and their connections [38].

In terms of the dynamical systems approach, we try to understand turbulence based on coherent structures. The term coherent structure has several meanings according to contexts. We use this term as a technical term of the dynamical systems approach. That is, coherent structures are supposed to be related to some characteristics of solutions to dynamical systems. Roughly speaking, coherent structures are minimal autonomous components of dynamic and vortex structures embedded in turbulence. In other words, an immediate objective of the dynamical systems approach in this thesis is to identify appropriate definition of coherent structures.

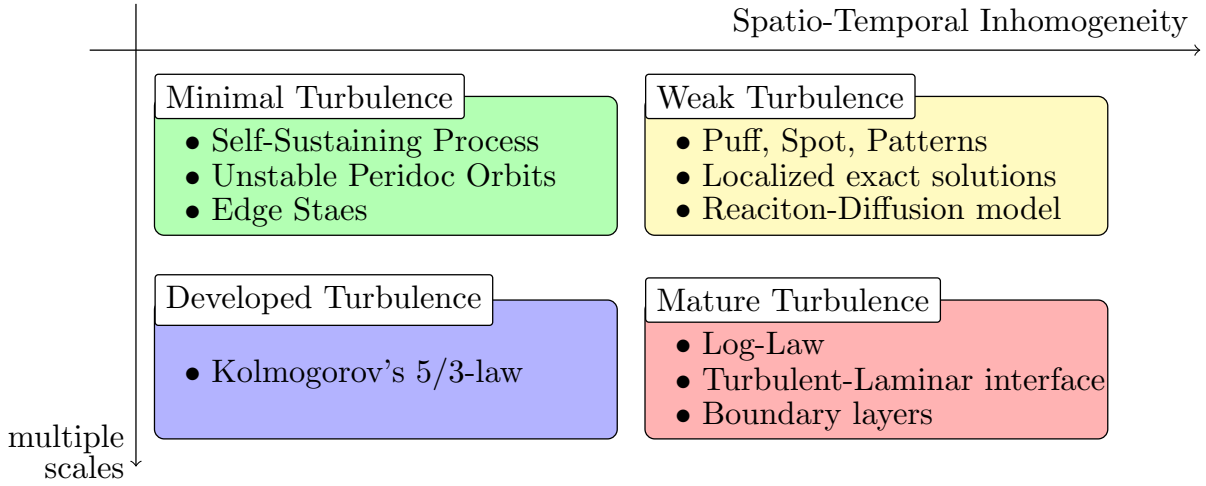

Figure 1.1: A rough categorization of turbulence matched to the development of the dynamical systems approach.

1.2 Dynamical systems approach to turbulence

In this section, we give a short review of the dynamical systems approach to turbulence by introducing four terms about turbulence (see Fig. 1.1). These terms are not widely used, but help us clarify the objective and problems of the dynamics systems approach.

1.2.1 Minimal Turbulence

Minimal turbulence denotes a temporally chaotic flow in a small periodic region. It is well known numerically that there is the minimal periodic domain of wall-bounded flows of which the statistical properties correspond to those of turbulence in large domains [6]. Numerical simulations of minimal flows yield low-dimensional nonlinear dynamics, i.e. fixed points, periodic orbits, period doubling sequence, and boundary crisis. The laminar state is stable at low Reynolds numbers, and thus these dynamics appear subcritically. We also call these low-dimensional dynamics minimal turbulence because they are embedded in turbulence and describe the characteristics of turbulence.

The studies for coherent structures using exact solutions have been developed with the minimal flow turbulence [6] by rephrasing the ideas in dynamical systems theories. Since the dynamics and spatial structures are strongly connected, invariant sets in the dynamical systems theories, e.g. fixed points, periodic orbits, and chaotic attractor, have corresponding structures. This correspondence is the basis of coherent structures. Especially, periodic orbits corresponding to periodic motions of coherent strucures, e.g. vortices and streaks in wall-bounded flows are useful since they can be treated statically. In other words, turbulence approximated by a closed cycle of coherent structures is statically represented by its correspondent periodic orbit. It is very powerful for both identifying and categorizing nonlinear dynamics. One important example of this correspondence is Waleffe's self-sustaining process (SSP) [14], corresponding to an unstable periodic orbit [17]. This periodic orbit describes the regeneration cycle of near wall turbulence made up with tilted vortices and a streak. Exact periodic solutions enable us to track how this

structure appears and when it becomes a chaotic saddle from the attractor as Reynolds number changes.

1.2.2 Weak Turbulence

We observe spatially extended, unsteady but not so active flows at relatively low Reynolds number where turbulence barely keeps alive. Here, we call these flows "weak turbulence" while this term has several meanings according to the context. The Reynolds numbers are below the critical Reynolds numbers of linear stability of the base flows, and thus these flows are bi-stable systems in this sense. These flows do not have continuous spatial scales different from developed and mature turbulence, so that they can be characterized with a few typical scales. Therefore, spatial inhomogeneity is expected to make the dynamics of the whole system high-dimensional while local dynamics seems to be low-dimensional. In this transitional parameter region, in fact, there exit various types of laminar-turbulence coexisting flows, e.g. puff, slug, spot, and stripes. One important objective is to understand this spatial inhomogeneity in terms of dynamical systems approach.

The studies about "weak turbulence" can be roughly categorized into two groups. One group has extended the approach that succeeded in minimal turbulence by obtaining various localized solutions to represent localized dynamics [26, 31, 33, 44]. These localized solutions show that the local dynamics in weak turbulence is quite similar to SSP in minimal turbulence. Comparing them with minimal turbulence in which the system is filled with turbulence, these localized solutions are isolated turbulent patches (see Fig. 1.4).

The other group has developed effective coarse grained models. There are several attempts to describe the spatial patterns in weak turbulence under the reaction-diffusion contexts [37, 43]. For representing the "reaction" component, some use the four-mode Galerkin approximations model [14] or the first model for SSP [11], and others more simplified modes. Locally bi-stable models, i.e. stable laminar and "turbulence" states, can describe the slug expansion process well. To explain the puff splitting process, Barkley et al.[37] introduced a stochastic transition from the "turbulence" to the laminar state. This model corresponds to the chaotic saddle creation in minimal flows [51]. These stochastic models are summarized into percolation models [25, 40, 41, 48], and well describe the transitional processes [23, 36]. These results indicate that the turbulence in the transitional parameter region can be represented by the combination of local or pointwise dynamics corresponding to SSP and its simple diffusive spatial interactions. In other words, Waleffe's SSP explains how the cite of percolation appears from the continuous systems. There are two simplifications: One is the low-dimensional models of local dynamics, and the other is the diffusive interactions among coherent structures. These simplifications seem to reflect the local low-dimensionality and weak inhomogeneity of near transitional flows.

1.2.3 Developed Turbulence

At relatively higher Reynolds number, the difference between the maximum and minimum scales in turbulence becomes wider, and the dynamics becomes multi-scale. Here, we in-

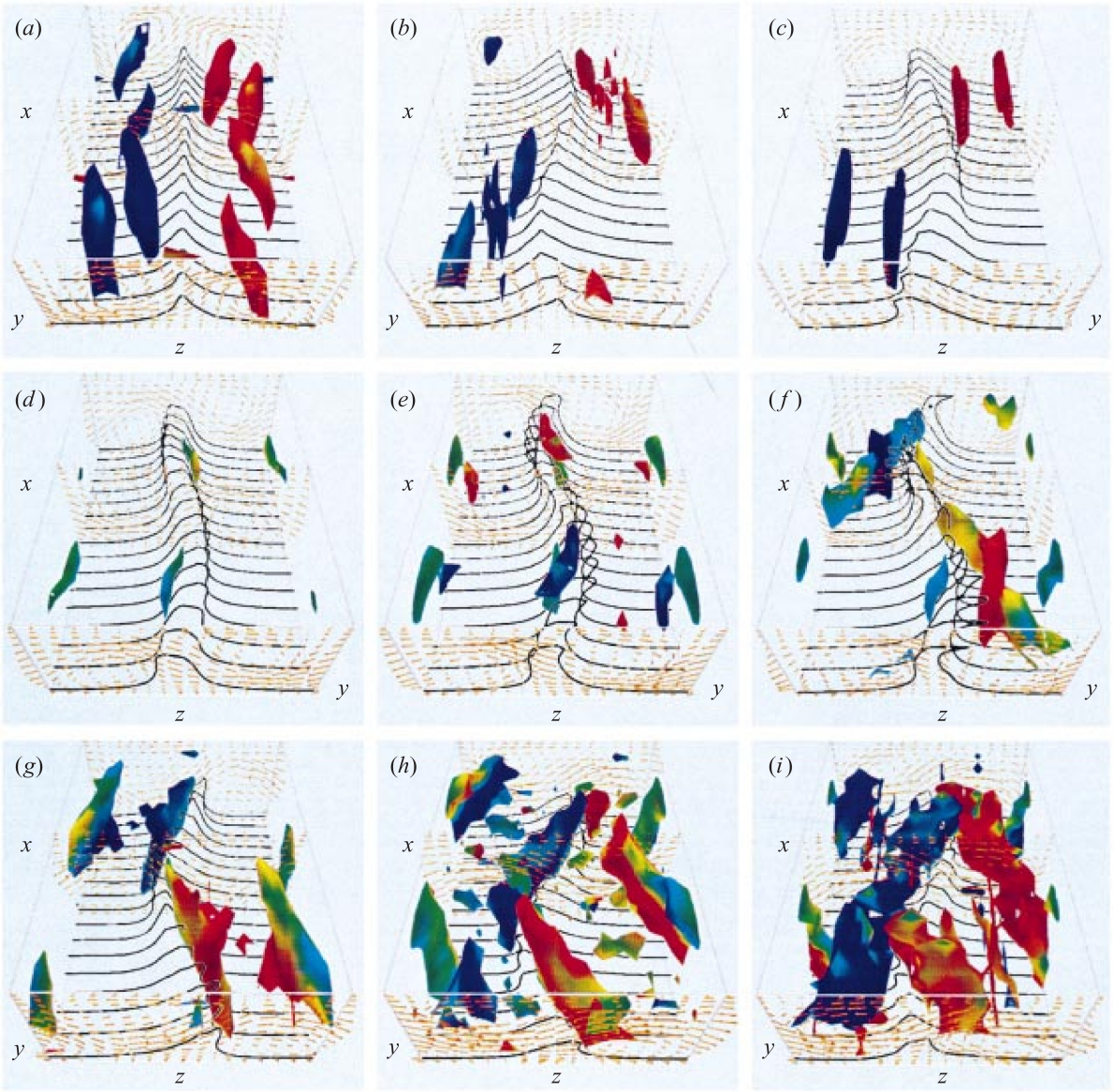

Figure 1.2: Cited from Kawahara & Kida, JFM (2001) [17]. Nine snapshots of unstable periodic orbit corresponding to SSP, the regeneration cycle of near wall turbulence.

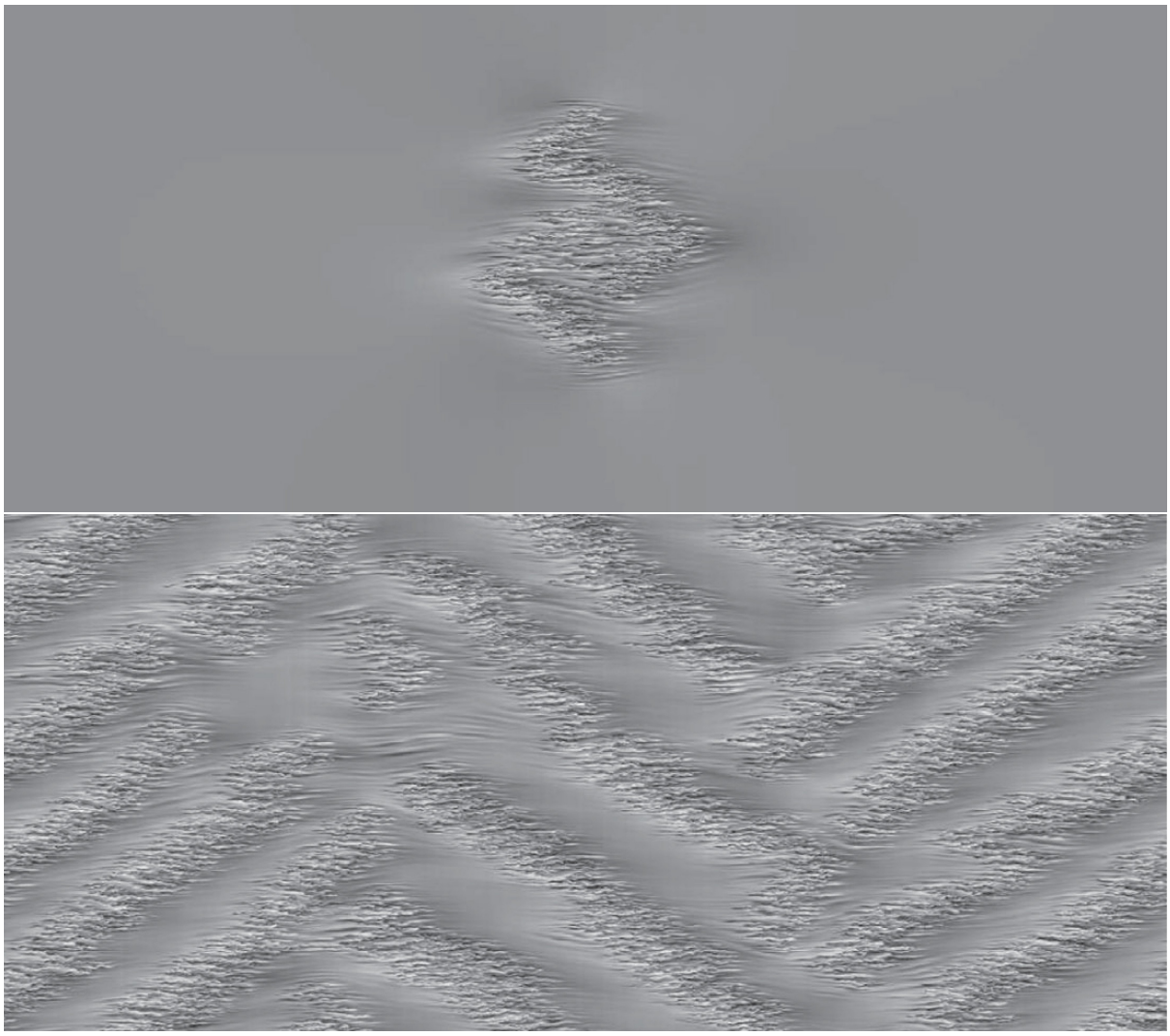

Figure 1.3: Cited from Duguet et al. JFM (2010) [34]. Turbulent spot (upper) and Turbulent pattern (lower) in simulations of plane Couette flow.

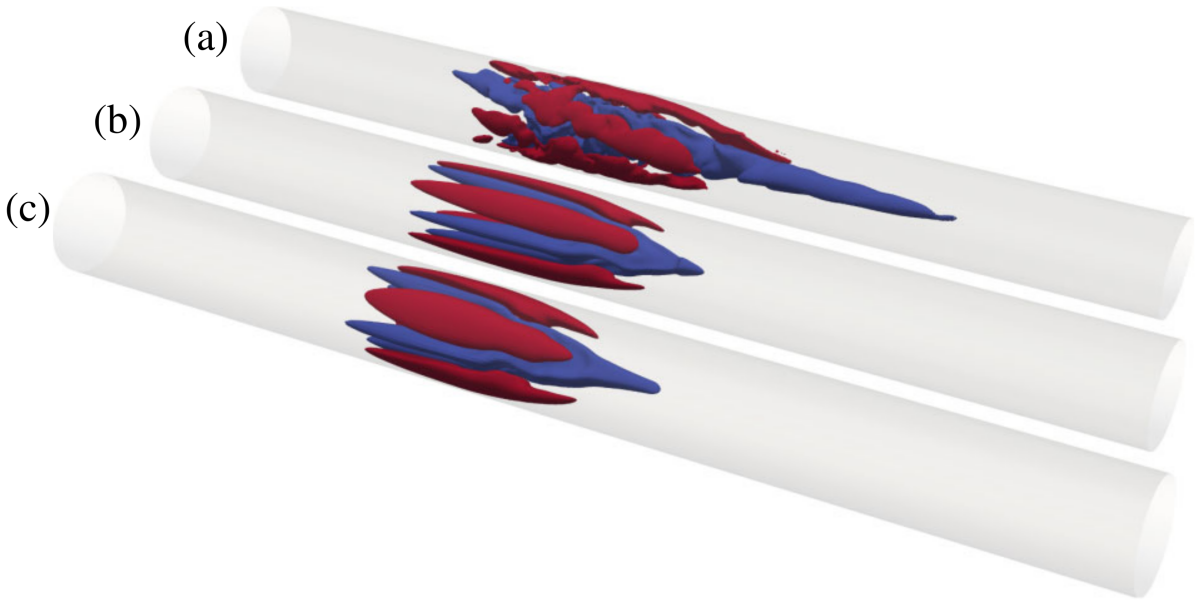

Figure 1.4: Cited from Avila et al. PRL(2013)[44]. Localized exact traveling-wave solutions and chaotic solutions in pipe flow.

troduce two terms, developed and mature turbulence to represent these spatio-temporally highly chaotic flows. We call multiscale uniform turbulence developed turbulence. It should be noted that uniform turbulence contains internal spontaneous inhomogeneity while long-time mean becomes uniform. In other words, we use the term developed turbulence if we focus on the multiscale property without inhomogeneity.

Large amounts of studies about turbulence have been devoted to statistical theories for developed turbulence. K41 model known as Kolmogorov's 5/3-law would be one of the most famous ones. Richardson's energy cascade picture describes the energy transfer from large scale vortices to small scale vortices. This picture introduces a fundamental energy transfer between vortices of adjacent scales. The energy cascade picture is widely accepted as a phenomenological explanation, but the spatio-temporal dynamics of this fundamental energy transfer is still hardly understood. Recent numerical analyses [28, 54] try to understand the dynamics of this fundamental process. The dynamical systems approach should be able to treat this problem. However, the current framework based on exact localized solutions is hardly adopted since it is incredibly hard to obtain localized exact solutions of this system.

1.2.4 Mature Turbulence

Turbulence in real world is further complex than developed turbulence defined above. Most turbulence have autonomous spatial inhomogeneity even in isotropic turbulence [32]. The intensities in active and inactive regions significantly differ, and a sharp interface is formed between them [46]. If a wall exists, the properties of turbulence in the boundary layer is neither isotropic nor uniform, and we usually have to consider flows around complicated walls or objects. So the real world turbulence is characterized by inhomogeneity and multiscaleness. To fill the gap between developed and real

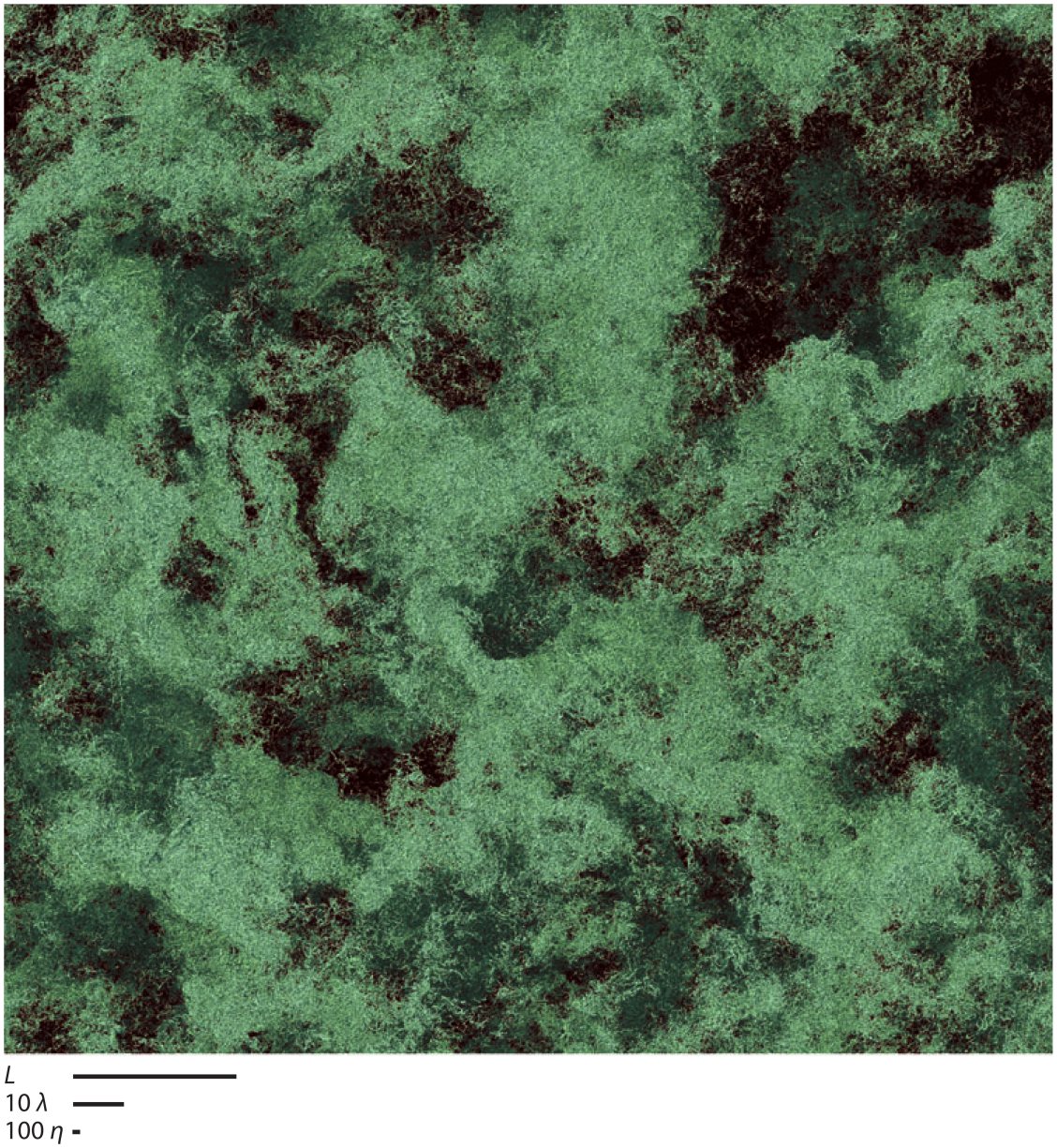

Figure 1.5: Cited from Ishihara et al. Annu. Rev. Fliud Mech. (2009) [32]. Spontaneous spatial inhomogeneity in isotropic turbulence. There are active and inactive turbulent regions.

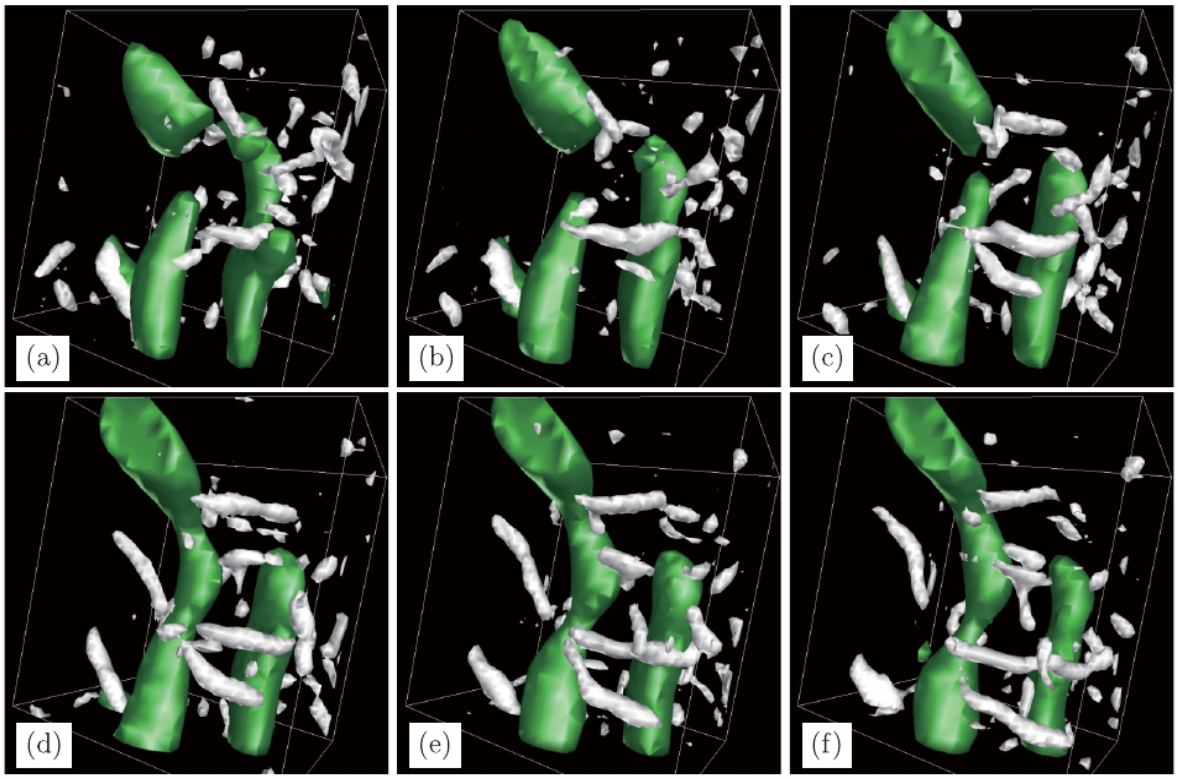

Figure 1.6: Cited from Goto, PTP (2012) [42]. Vortex structures of fundamental process of Richardson's cascade.

world turbulence, we introduce a class of turbulence to focus on the inhomogeneity which cannot be represented as weak turbulence, and call it mature turbulence.

For example, we include statistically steady wall-turbulence dominated by the log-law in mature turbulence because of its spatial inhomogeneity in the wall-normal direction. Fundamental processes of the log-law in wall turbulence have been discussed based on the classical mixing length theory, which introduces hypothetical vortices to understand the momentum transfer from the bulk to the wall. In the engineering context, some parts of these processes are approximated into the eddy viscosity model, so that the effect of these fundamental processes are reduced to the correction of the viscosity coefficient. Other studies, e.g. free shear flow approximations [49], and the vortex wave interaction theory [47] try to obtain coherent structures corresponding to this hypothetical vortex. These studies suggest that the log-law can be understood by the hierarchal collective dynamics of coherent structures corresponding to fundamental mixing processes. This hierarchal property is similar to the Richardson's cascade in developed turbulence, but in this case the properties of coherent structures differ according to their positions; near wall vortices are small and far wall vortices are large. In other words, mature turbulence is characterized by spatially segregated different coherent structures. Such collective dynamics significantly differ from the diffusive connection appeared in weak turbulence. The framework used in the studies of weak turbulence, i.e. diffusive connection between coherent structures, seems not to be able to treat these "functional" corporation of coherent structures: The fundamental coherent structure of log-law will have a function of momentum transfer, and that of Richardson's cascade will have a function of energy transfer. These functions should be responsible not for the interaction among them but for each coherent structure, and thus we call them "functional coherent structures". A simple example of mature turbulence is introduced in Chapter 3. Such complex functionality of coherent structures seems to appear at larger Reynolds number, and then the dynamics of mature turbulence must be multiscale.

Comparing developed and mature turbulence, mature turbulence may be more complicated. However, a model that we introduce in Chapter 3 to represent a functional corporation of coherent structures should be included in mature turbulence. Spatial inhomogeneity rather helps us separate the dynamics of coherent structures. Considering coherent structures in mature turbulence will be a possible path of the extension of the dynamical systems approach to developed turbulence.

1.3 Outline

As discussed above, the current dynamical systems approach based on exact solutions can be adopted to weak turbulence, but cannot be applied to developed and mature turbulence. This thesis makes two attempts:

- Chapter 2: We extend the exact solution based approach to mature turbulence
- Chapter 3: We introduce a new framework, "functional coherent structure" instead of the exact solution based one.

Both of two attempts are based on a common technique called a damping filter method in which a damping filter term is introduced to the equation of motion.

In Chapter 2, we introduce a novel efficient methodology to obtain localized exact solutions. This study extends the localized exact solution approach in weak turbulence to mature turbulence. In weak turbulence, localized pointwise dynamics is minimal turbulence, whose properties are well studied in minimal flow simulations. However, localized dynamics in mature turbulence does not have corresponding minimal flow because various coherent structures will only appear as a part of mature turbulence. This method gives an efficient way to split out such coherent structures as localized exact solutions, which contain abundant information about the local dynamics.

In Chapter 3, we focus on a turbulent-laminar interface structure in two-dimensional channel flow. Since we deal with flows at relatively high Reynolds number, $Re = 6000 \rightarrow 10000$, the laminar flow is unstable, and turbulence invades the laminar part. This transient process is kept permanent using damping filter technique. It is shown here that this system is included in mature turbulence. There is a self-sustaining coherent structure in the interface region, and it transfers energy from the laminar part to a following weak turbulence part. The self-sustaining mechanism of this functional coherent structure is summarized into a phenomenological model, we call ejection-jet cycle.

In the last chapter, we give a comprehensive discussion how these two approaches extend the current framework of coherent structures. We also summarize and conclude this thesis comprehensively.

Chapter 2

Damping filter method

2.1 Introduction

There exist various types of localized structures. For example, turbulent puffs in pipe flow are localized in the stream-wise direction; turbulent spots in channel flow do both in the stream-wise and span-wise directions. If there exists a solution corresponding to large scale motions, it will be localized in the wall-normal direction. In this paper, we focus on the two typical cases both of which will be instructive in understanding localized structures observed in turbulence. We show not only basic usage and results but also remarkable features of our method in Sections 2.3 and 2.4.

We first consider localized solutions to Swift-Hohenberg equation (SHE) [24, 29, 30]. This is a representative example of localized solutions in bi-stable systems. This class of localized solutions contains, for example, span-wisely localized solutions corresponding to roll-streak structures in plane Couette flow [35]. Their solution branches are very similar to the "snaking" branches seen in SHE [24]. Similar structures of solution branches are also found in doubly diffusive convection systems [27]. These facts indicate that there exists a universal mechanism of spatially localized solutions in the bi-stable systems. We deal with solutions in this class in Section 2.3.

Second, we examine a spatially localized traveling-wave solution to Kuramoto-Sivashinsky equation. Such a solution can be regarded as a stream-wisely localized solution. Stream-wisely localized structures can be observed in pipe flow (turbulent puffs), boundary layers (hairpin vortexes), and so on. The sustaining mechanism of them might be different from that of span-wisely localized solutions, and thus it is necessary to obtain the corresponding solutions in order to analyze them from a dynamical systems viewpoint. At a glance, since our method utilizes a spatially selective damping effect that breaks translational invariance, it seems to have only limited capability for this issue. However, we show that this is not the case in Section 2.4.

This chapter is organized as follows. In Section 2.2, a damping filter method is introduced, where we explain its concept and concrete procedure. In Sections 2.3 and 2.4 we adopt the method to Swift-Hohenberg equation and Kuramoto-Sivashinsky equation respectively in order to obtain spatially localized solutions. Finally, this paper is concluded with concluding remarks in Section 2.5.

2.2 Numerical Procedure

In this section the protocol of the damping filter method is explained. This method consists of three steps. Since this method can be used for various systems, a general form evolution equation, $\partial_t u = F[u]$, is used in the following explanation.

The first step of this method is to introduce a spatially selective damping term into the evolution equation. The damping term works only in a region Ω. If we want to obtain a span-wisely localized solution, Ω should be a region localized in span-wise direction. If we want to obtain a solution localized like turbulent spot, Ω should be a spot region. Then the damping term is introduced as follows:

$$\partial_t u(x,t) = F[u](x,t) - A_f H(x) u(x,t). \tag{2.1}$$

We call this equation "filtered equation" hereafter. The damping term consists of the filter amplitude A_f and a filter function $H(x)$. $H(x)$ is defined to be zero in the region Ω and to be 1 out of Ω, and smoothed by taking a convolution with a mean-zero Gaussian $\mathcal{N}_{0,\sigma^2}(x)$ in order to avoid the numerical singularity:

$$H(x) = \int \mathcal{N}_{0,\sigma^2}(x-y)\hat{H}(y)dy, \tag{2.2}$$

$$\hat{H}(x) = \begin{cases} 0 & (x \in \Omega) \\ 1 & (x \notin \Omega) \end{cases}. \tag{2.3}$$

The integral is taken in the whole region. The damping term causes a linear damping effect out of Ω (filtered region), and the filtered equation equals to the original equation $\partial_t u = F[u]$ in Ω (unfiltered region).

The second step is to obtain an exact solution to the filtered equation (2.1). Owing to the spatially selective damping effect, the direct numerical simulation (DNS) of the filtered equation tends to yield a spatially localized time series $u(x,t)$, in other words, $u(x,t)$ decreases exponentially fast as x goes away from Ω after a relaxation time. In addition, since the damping effect weakens the instability of the system, DNS sometimes yields a non-trivial stable solution for enough large filter amplitudes and an appropriate Ω. In this case the second step is finished with this stable solution. If any stable solutions are not obtained, a solution to the filtered equation is obtained by solving an equation $F[u] - A_f H(x) u = 0$ about $u(x)$ with Newton method. Since the degree of freedom is also reduced by the damping term, it is expected that such a solution can be obtained easily.

The third step is a continuation process. The solution obtained in the second step depends on the filter amplitude A_f, and often this dependency is continuous. A continuation with A_f is started from this solution. The filter amplitude A_f is decreased until it gets to zero, where the filtered equation is restored to the original equation in the whole region. Then the continuated solution is nothing but that to the original equation. This is the goal of the damping filter method. The continuation is implemented by the arc-length method with Newton-Krylov iterative method, and thus applicable to systems having large degree of freedom.

The good feature of our method is that an appropriate guess of a spatially localized solution is constructed as a solution to the filtered equation (2.1). This guess reflects

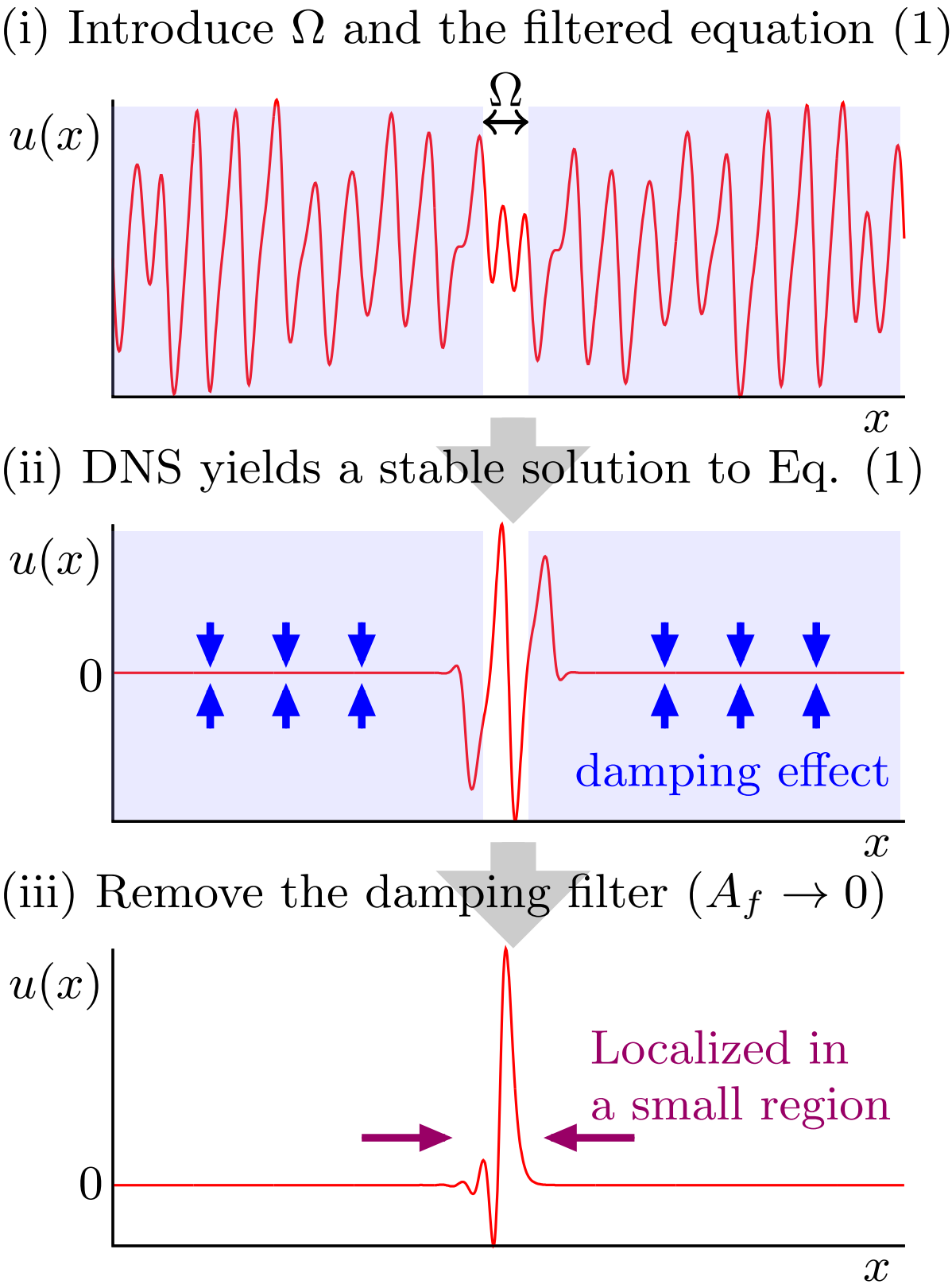

Figure 2.1: (Color online) Three steps in the damping filtering method.

the dynamics of spatially localized structures since the filtered equation equals to the original equation in the region Ω. In another study [5], an artificial external forcing is used for constructing a guess of solutions. It was designed by hand from the inference about the dynamics of localized structures. In our method such artificial manipulation is not needed except for determining the region Ω.

This spatially selective damping is inspired by the work [16]. They have investigated an autonomous behaviors of near-wall structures by a filtered dynamics. In contrast to them, our method uses this filtered dynamics only for guesses and continuations, and removes the filter finally. Thus, our method enable us to study the non-filtered dynamics by localized solutions.

2.3 Span-wisely localized solutions

In this section we consider one-dimensional Swift-Hohenberg equation (SHE):

$$\frac{\partial u}{\partial t} = F[u] = \left(r - \left(\frac{\partial^2}{\partial x^2} + 1 \right)^2 \right) u + 2u^3 - u^5. \tag{2.4}$$

As noted in the introduction, a series of solutions to SHE is regarded as a representative of localized solutions in the bi-stable systems. The following subsections show two things: (i) We can obtain span-wisely localized solutions by our method. In order to show this, we reproduce solutions belonging to the homoclinic snaking branches. The practical detail of our method is also described. (ii) Our method has a capability for obtaining various solutions that are usually hard to be found. Indeed, we find an isolated and closed solution branch. Since isolated solution branches cannot be found by the weakly nonlinear framework, this success indicates an advantage of our method.

2.3.1 Homoclinic snaking branches

In this subsection we apply our method to SHE in order to obtain a localized steady solution belonging to the snaking branches. Although the branches contain stable localized solutions for a parameter region, the attracting basins of them are very small, and thus it is almost impossible to obtain these localized solutions by DNSs with arbitrary initial conditions.

Before adopting our method, the setting of system is described. We consider SHE in a region $[0, L], L = 180$, and impose a fixed boundary conditions $u(0) = u(L) = 0$. The parameter r is set to -0.669 in this subsection, and -0.633 is used in the next subsection. Time evolutions are solved by the quasi-spectral method with the classical fourth-order Runge-Kutta method. We regard a steady point of DNS as a steady solution to the equation, so the DNS code is used also in continuation processes.

We describe the practical details of our method hereafter. The first step of our method is to introduce the damping term. The unfiltered region Ω is set to be $[80, 100]$, and the filter function $H(x)$ is smoothed with $\sigma^2 = 0.01$. The amplitude of the filter A_f is set to be 1.

The second step is to obtain an solution to the filtered equation (2.1) with $F[u]$ of Eq. (2.4). This equation has a stable localized steady solution with these parameters. The

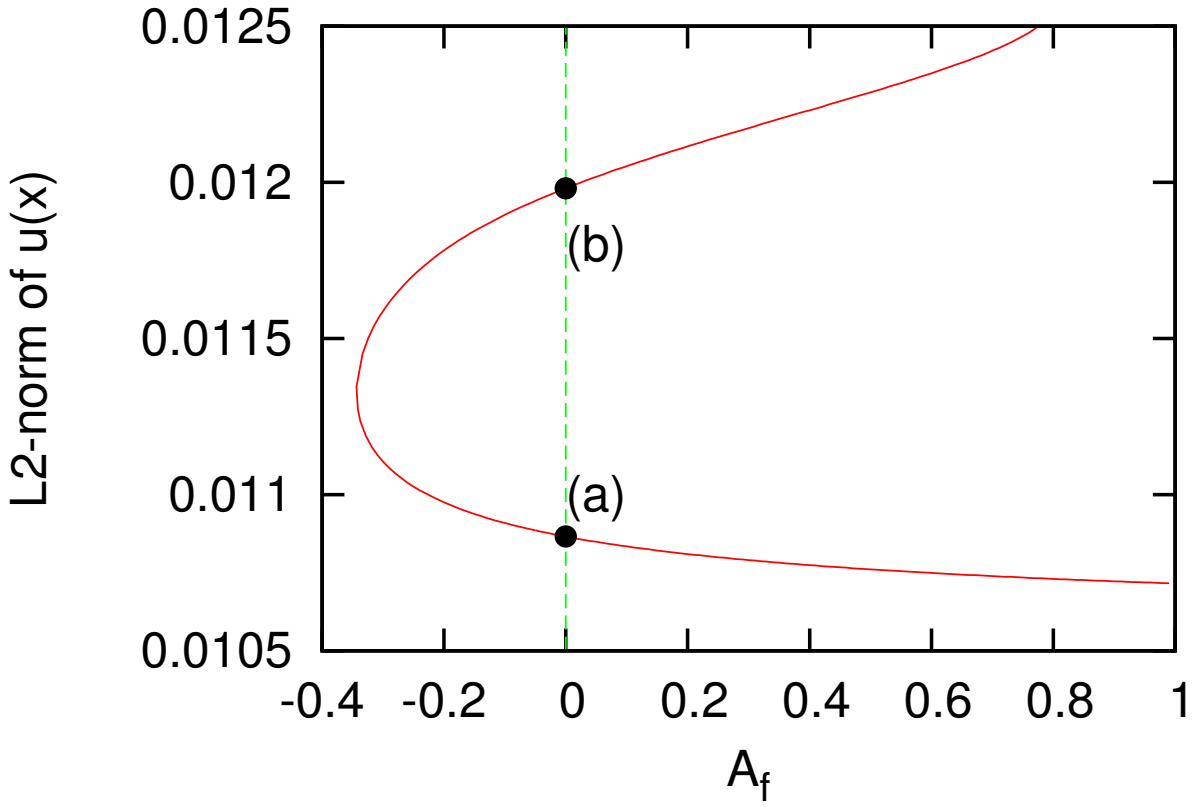

Figure 2.2: (Color online) The trajectory of continuation projected onto a A_f-$\|u\|$ space. Each of two labeled solutions (a),(b) on the line $A_f = 0$ denotes a solution to SHE. The continuation is continued after the filter amplitude A_f became zero, and yield a solution labeled (b). The profile of these solutions are shown in Fig. 2.3.

initial condition of this DNS is the stable steady sine-like solution of non-filtered equation (2.4), which is not spatially localized but spatially extended. Such a localized solution to the filtered equation exists while $r \lesssim -0.72$. This lower limit almost agrees with that of the snaking branches. Since the spatial period of the sine-like solution is 2π, these localized solutions to the filtered equation contain almost three periodic components.

The third step is a continuation process. The parameter traced in this continuation is the filter amplitude A_f, and the parameter r is fixed. The result of the continuation is shown in Fig. 2.2, which displays the trajectory of the continuation projected onto a A_f-$\|u\|$ plane. Here $\|\cdot\|$ denotes the L^2-norm. The trajectory crosses the line $A_f = 0$ twice. Although a solution to SHE is obtained when the trajectory crosses the line first and thus the damping filter method finishes at this time, we find that the trajectory turns back and crosses the line $A_f = 0$ again. Eventually, we successfully obtain two solutions to SHE, and the profile of them are shown in Fig. 2.3. These solutions are localized almost in $[70, 110]$, which is larger than $\Omega = [80, 100]$. This fact indicates that Ω is only a guide for obtaining a spatially localized solution, which obeys not the damping filter but the original equation.

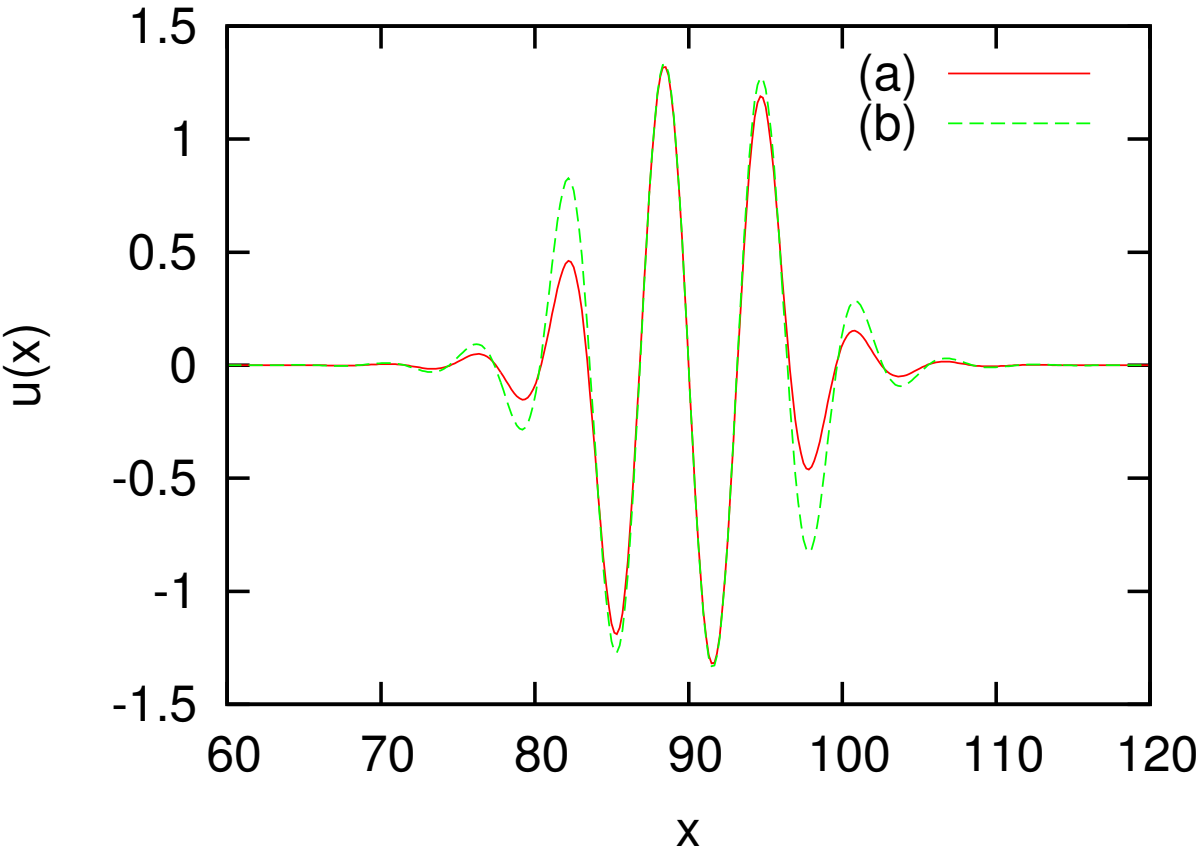

Figure 2.3: (Color online) The profiles of the solutions obtained in the continuation shown in Fig. 2.2. Since the tails of the solutions decay exponentially, These solutions are localized almost in $[70, 110]$, and have an exponentially decaying tail.

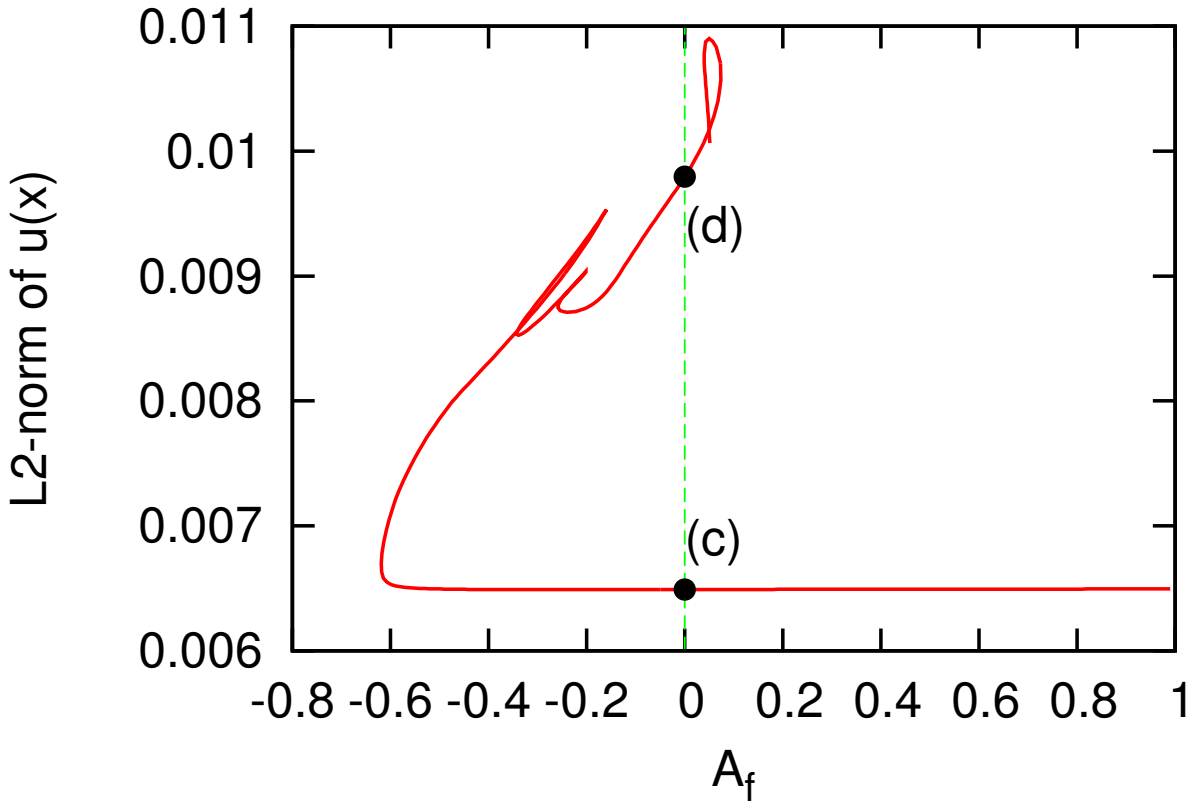

Figure 2.4: (Color online) The trajectory of continuation projected onto A_f-$\|u\|$ started from an unstable solution to the filtered equation. This continuation also cross the line $A_f = 0$ twice, but a complicated path is realized. Two labeled points (c) and (d) on the line $A_f = 0$ are also solutions to SHE, and their profiles are shown in Fig. 2.5. As noted in the text a switching between solution branches are occured in this complicated part of the trajectory.

2.3.2 An isolated closed branch

We execute the same procedure for various values of the parameter r. For most of r it yields continuation trajectories and solutions to SHE similar to those shown in the previous section. However, we also find quite different behaviors in some cases, one of which we focus on in this subsection.

As an initial guess we use a solution to the filtered equation obtained by a continuation with the parameter r started from the solution to the filtered equation used in the previous section. The other parameters are same as those of the previous section: $\Omega = [80, 100]$ and $A_f = 1$.

The result of the continuation with A_f starting from this starting solution is displayed in Fig. 2.4. Compared with Fig. 2.2, the continuation trajectory is very complicated especially in the region $A_f < 0$. The two solutions on the line $A_f = 0$ are labeled as (c) and (d), and their profiles are displayed in Fig. 2.5.

A difference between the solutions (c) and (d) can be observed in its profile: The solution (c) is a single pulse solution like the solutions (a) and (b). On the other hand, the solution (d) seems to be a combination of two antisymmetric pulse solutions. There

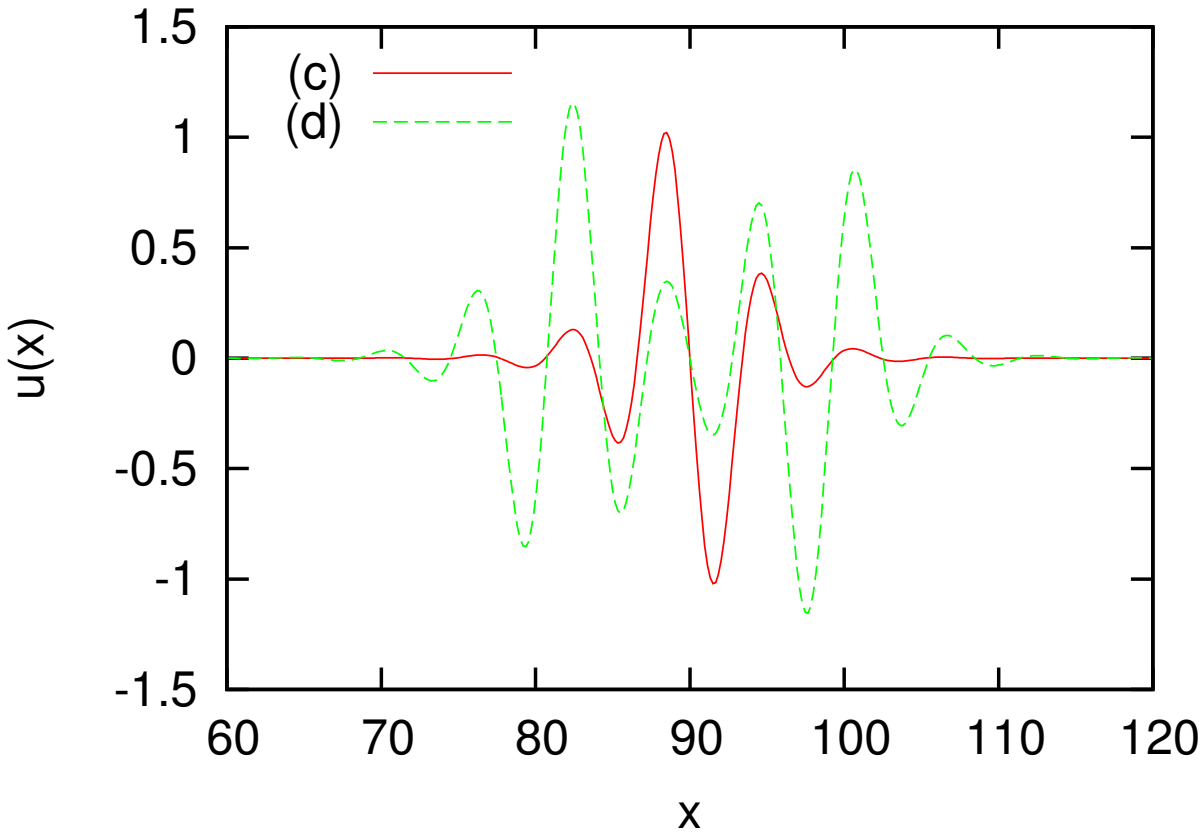

Figure 2.5: (Color online) The profiles of the solutions (c) and (d). In contrast to Fig. 2.3, the profiles of the solutions (c) and (d) are qualitatively different.

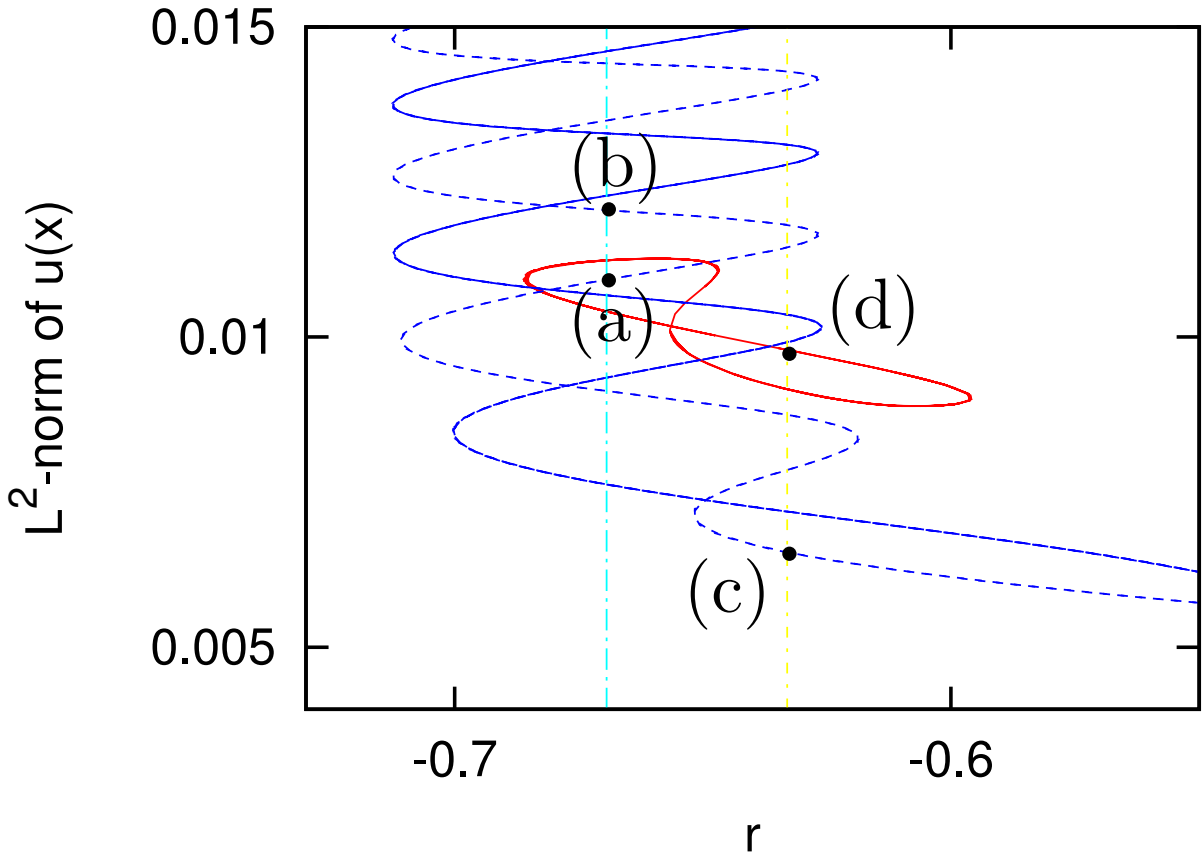

Figure 2.6: (Color online) The snaking branches and isolas projected onto a r-$\|u\|$ plane. The snaking branches consist of two coupled branches, and solutions (a), (b) and (c) belong to the same one of them (dashed blue line). The red (dark gray) figure-eight shaped line denotes the isolas containing the solution (d). Such eight-figured branches can be seen also in two-pulse solutions to SHE [39]. This similarity tells that the solution (d) should be regarded as a connected two-pulse solution.

exists the definitive difference in their solution branches as shown in Fig. 2.6. This figure shows that the solutions (a), (b), and (c) belong to the snaking branches, but the solution (d) belongs to an isolated closed branch. Such closed isolated solution branches are called "isolas" in [39].

It should be noted that two distinct branches are connected by the continuation with A_f. Moreover, they connect through the region where A_f becomes negative, where the term $-A_f H(x)u$ works as an excitation term. Thus the connection can be regarded as a result of the instability caused by this term. Since $u(x)$ has an exponentially decaying tail, this instability occurs only around the edge of Ω. So this linear exitation is also spatially selective.

2.4 Stream-wisely localized solutions

In this section a stream-wisely localized solution, in other words, a solution localized in its moving direction is studied with Kuramoto-Sivashinsky equation (KSE):

$$\frac{\partial u}{\partial t} = F[u] = -u\frac{\partial u}{\partial x} - \frac{\partial^2 u}{\partial x^2} - \frac{\partial^4 u}{\partial x^4}. \tag{2.5}$$

It should be noted that KSE has no localized equilibrium solution whose tail decays exponentially. If we adopt our method to Eq. (2.5), the continuation about A_f yields the flat solution $u = 0$ before A_f reaches zero. So we seek a stream-wisely localized traveling-wave solution (TWS) such that $u(x,t) = \hat{u}_0(x - ct)$ satisfying boundary conditions

$$\hat{u}_0(x - ct \to \pm\infty) \to 0.$$

In contrast to the case of span-wisely localized solutions, there are two issues in this case: One is a treatment of the propagation velocity of the solution, and the other is a breakdown of the localization. These issues will arise in more general cases since they are based on Galilean and translational invariances. In the following subsections a solution to these issues are described.

2.4.1 A treatment of the propagation velocity

Since a TWS travels downstream, its localized region must accompany. In order to obtain a localized TWS by our method, it is necessary to introduce a moving damping filter or a steady damping filter in a moving frame, and we chose the latter. Then the equation becomes as follows:

$$\frac{\partial \hat{u}}{\partial t'} = -(\hat{u} - c)\frac{\partial \hat{u}}{\partial x'} - \frac{\partial^2 \hat{u}}{\partial x'^2} - \frac{\partial^4 \hat{u}}{\partial x'^4} - A_f H(x')\hat{u}, \tag{2.6}$$

where $x' = x - ct, t' = t, \hat{u}(x', t') = u(x, t)$. We seek a steady solution satisfying $\partial_{t'}\hat{u} = 0$ in this frame. However, the velocity of the moving frame c is unknown unless the solution is obtained. Since KSE does not allow their solutions to continuously depend on c, a specific value c_0 with which a solution $\hat{u}_0(x - c_0 t)$ exists must be determined simultaneously.

Such a situation sometimes occurs when obtaining a TWS to an equation $\partial_t u = F[u]$. In these cases, this problem is usually resolved by regarding c as an unknown variable, and solving $-c\partial_x u = F[u]$ for $u(x)$ and c. Since the translational invariance reduces the degree of freedom, this simultaneous equation can be solved. In our method, however, the damping filter breaks Galilean and translational invariances, thus the usual technique cannot be adopted.

Although TWSs to KSE do not continuously depend on c, our results show that TWSs to the filtered equation do. This fact reflects the breaking of the translational invariance by the filter. The details are discussed in the last part of this section. Thus the propagation velocity c becomes one of the control parameters of the solution and can be chosen arbitrarily in a certain range. See also schematic view in Fig.2.7.

Then the other issue arises; how do we obtain the specific value c_0? Although there is a range of c in which the solution exists continuously, this range becomes narrower and narrower as A_f goes to zero, and finally converges to a point on $A_f = 0$. We get over this

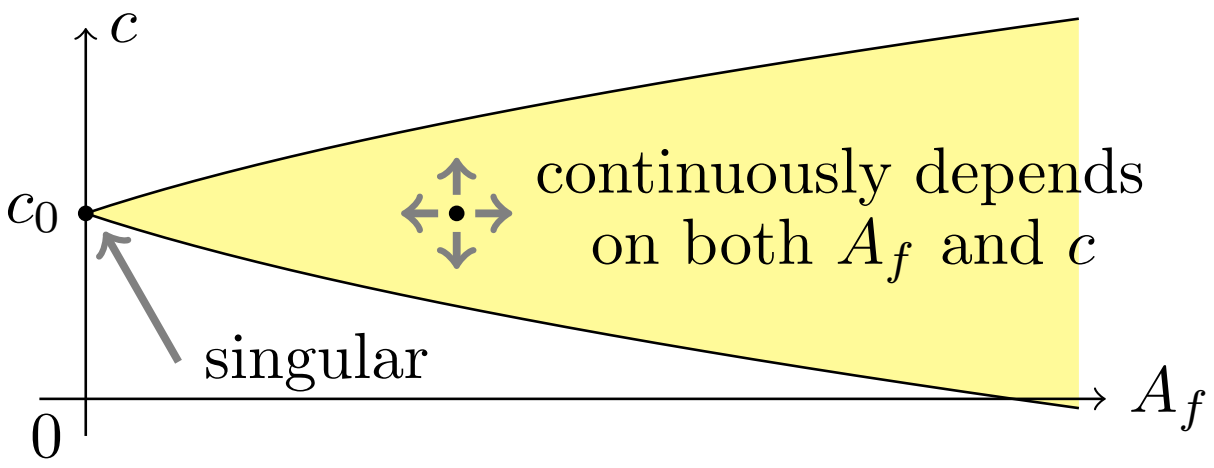

Figure 2.7: (Color online) An image for the continuous existence of solutions and singularity at $A_f = 0$. The existence of the solution is displayed in A_f-c plane. The solution exists continuously on the yellow (thin gray) crosshatched region, and cannot be traced beyond its rim. There is no guarantee that this solution branch connects to the line $A_f = 0$. If it does, only a point is allowed because the solution cannot exist continuously on the line $A_f = 0$.

issue by imposing an implicit relationship between c and A_f. This technique to impose the restriction is a key point to obtain a stream-wisely localized TWS. The details are discussed in the next subsection with our data.

2.4.2 Adopting the damping filtering method to KSE

In the first step of the damping filtering method, a localized region Ω is determined. We set the system size to $L = 200$ and the localized region $\Omega = [97, 103]$ in order to obtain a one-peak TWS. The filter function $H(x)$ is smoothed by Gaussian with $\sigma^2 = 0.01$ and the filter amplitude A_f is set to 4.8.

In the second step, a solution to the filtered Eq. (2.1) is obtained to start the continuation. As notated in the previous subsection, we can choose an arbitrary propagation velocity c in a certain range, and we choose $c = 0$ here. We execute a DNS of non-filtered equation (2.6) to produce a spatio-temporal chaotic field, which is used for an initial condition of a DNS of Eq. (2.6). This yields a stable solution, which is labeled as (a). These DNSs are solved by the quasi-spectral method with the classical forth-order Runge-Kutta method. Although a localized solution has an exponentially decaying tail and does not get exactly to zero in a finite distance, we regard small values comparable to the truncation error as zero and assume that the fixed boundary conditions $u(0) = u(L) = 0$ are satisfied. We use sine transform to ensure this condition with $N = 2048$ modes.

The third step is a continuation process. Since the propagation velocity c becomes a continuous parameter of the solution on $A_f > 0$ region, this continuation becomes essentially two-dimensional. It is almost impossible to obtain a full two-dimensional solution branch because of the numerical cost, we introduce a path on A_f-c space as follows.

As noted above, if c is fixed to zero then a continuation with A_f yields the flat solution

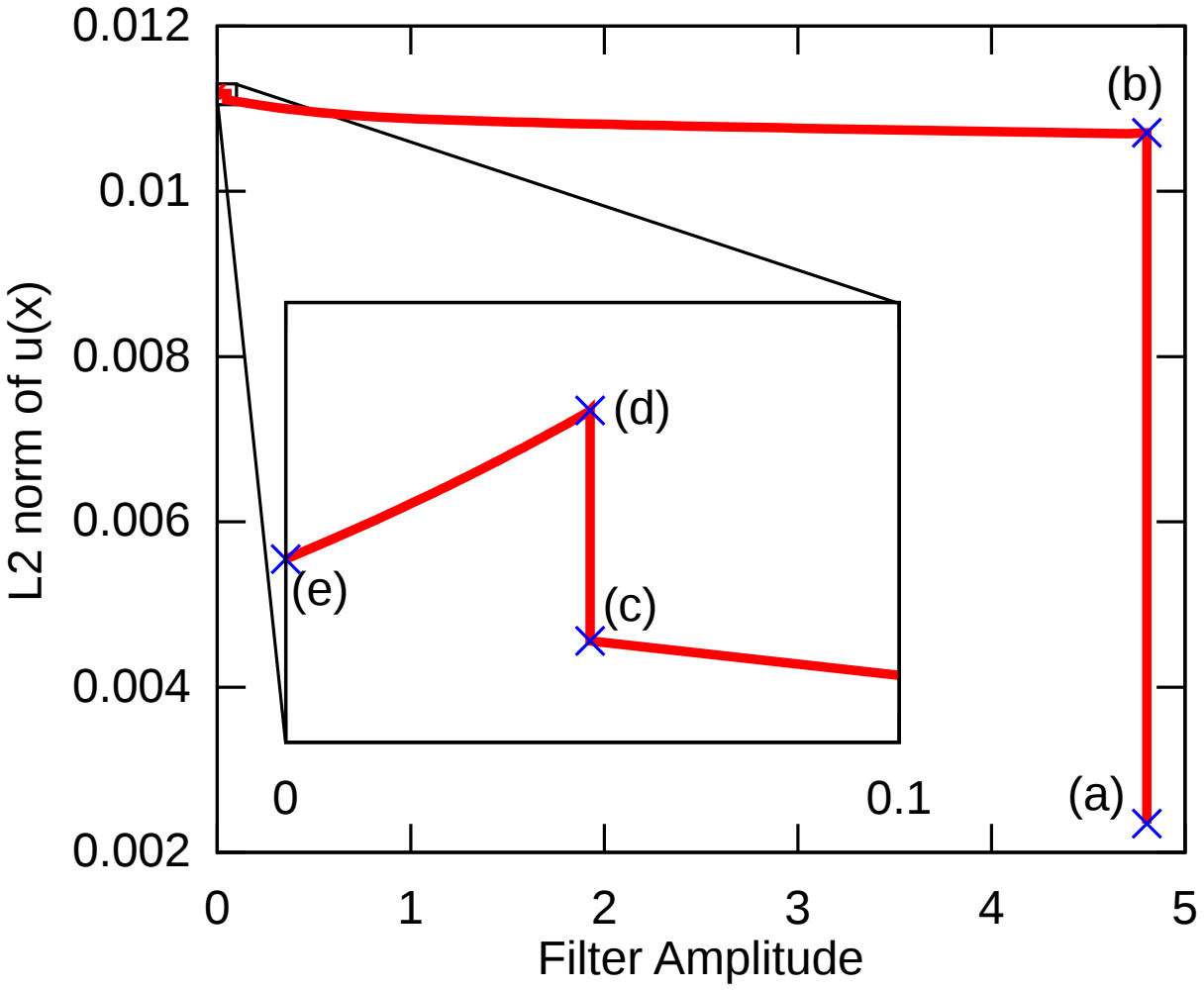

Figure 2.8: (Color online) The trajectory of the continuation projected onto A_f-$\|u\|$ plane. A closeup around $A_f = 0$ is also shown.

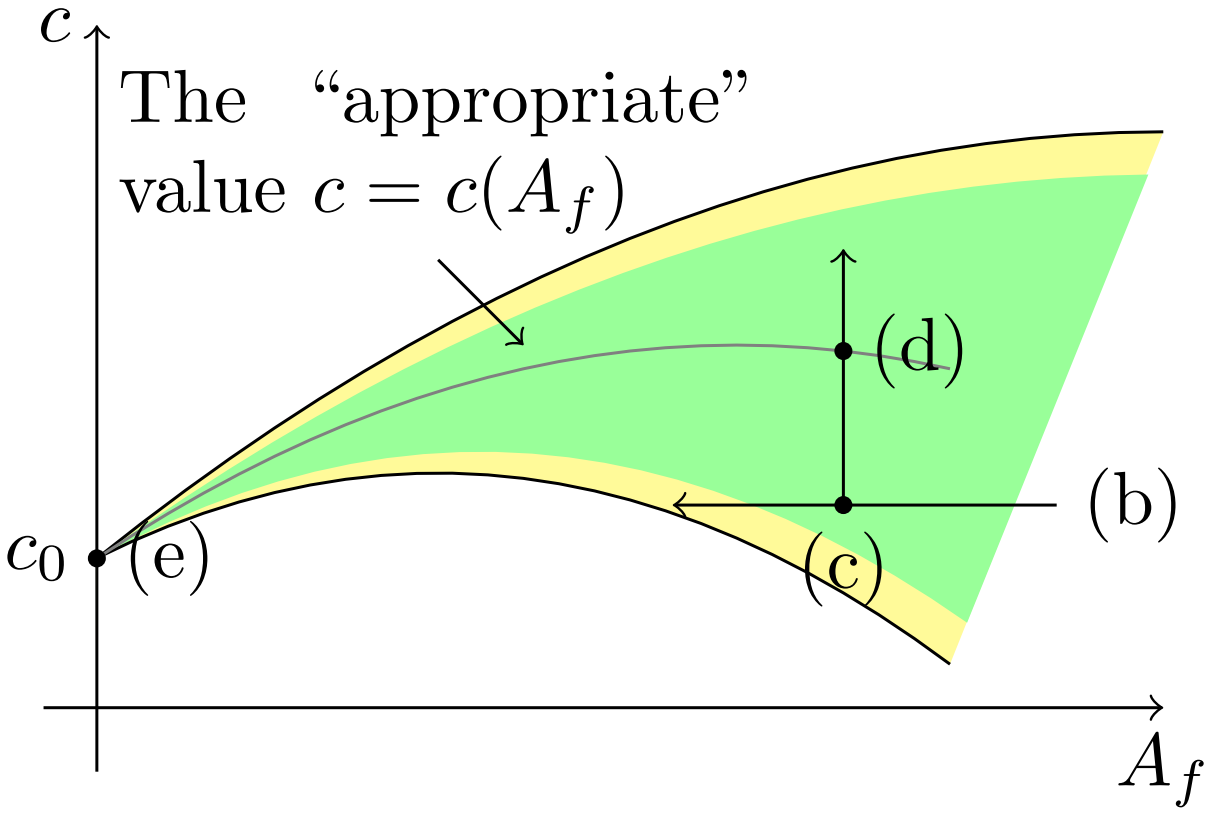

Figure 2.9: (Color online) An schematic view of the parameter dependency of the solution around $A_f = 0$. The yellow (thin gray) crosshatched region denotes one where a solution continuously exists, and the green (thick gray) region denotes one where a "localized" solution continuously exists. Here a "localized" solution means that it does not have the oscillation around the boundary. The three steps are as follows: (i): (b) $\to$ (c), (ii): (c) $\to$ (d), (iii): (d) $\to$ (e).

$u = 0$ before A_f reaches zero. In order to avoid this dead end, we first fix A_f to 4.8 and execute a continuation with c. The solution is traced up to $c \simeq 1.21$, which is labeled as (b). This value of c is determined by trial and error here, but a more practical criterion will be discussed in a future work.

The following continuation procedure is delicate because the uniqueness of the propagation velocity c must recover when $A_f = 0$. In short, the procedure consists of three steps (see Fig. 2.9): (i) A_f is reduced around 0.05 while c is fixed. (ii) A_f is fixed and c is adjusted to an "appropriate" value $c = c(A_f)$. (iii) c and A_f are traced simultaneously keeping the "appropriate" condition $c = c(A_f)$.

In the step (i), we fix c to 1.21 and execute a continuation with A_f. This continuation leads A_f around 0.01, but A_f cannot reach 0. In this continuation the profile of the solution changes as shown in Fig. 2.10. We define a characteristic length of the tail of the solution as the inverse of its decaying rate. As A_f decreases, it becomes longer and an oscillation starts to appear around the left boundary. If this tracing is continued further, the oscillation grows up and the solution may not be kept localized. Such non-localized solutions also cannot be traced till $A_f = 0$. This shows that a localized TWS to KSE cannot be obtained using only the continuation with A_f.

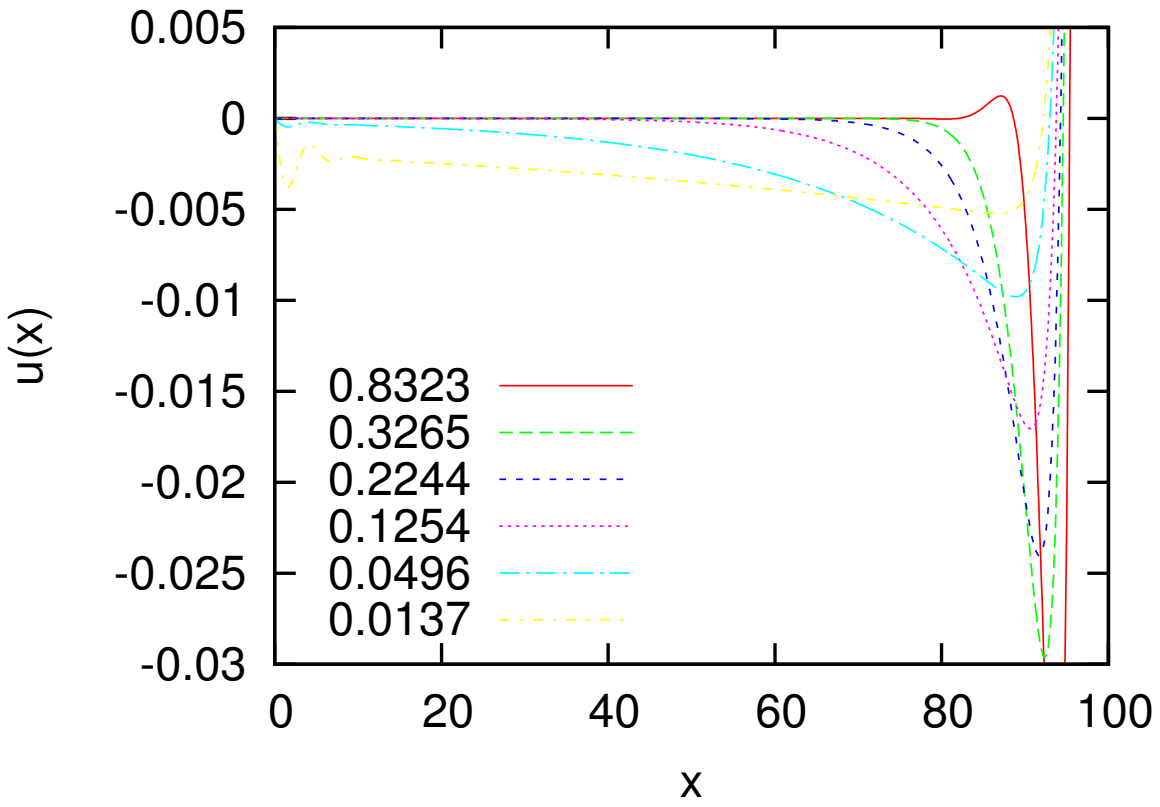

Figure 2.10: (Color online) The left tails of the solutions obtained while the tracing (b) to (c) whose A_f is 0.8323, 0.3265, 0.2244, 0.1254, 0.0496 and 0.0137 respectively. As A_f decreases, the characteristic length of the tail becomes longer and longer. Finally an oscillation appears around the left boundary due to the boundary condition.

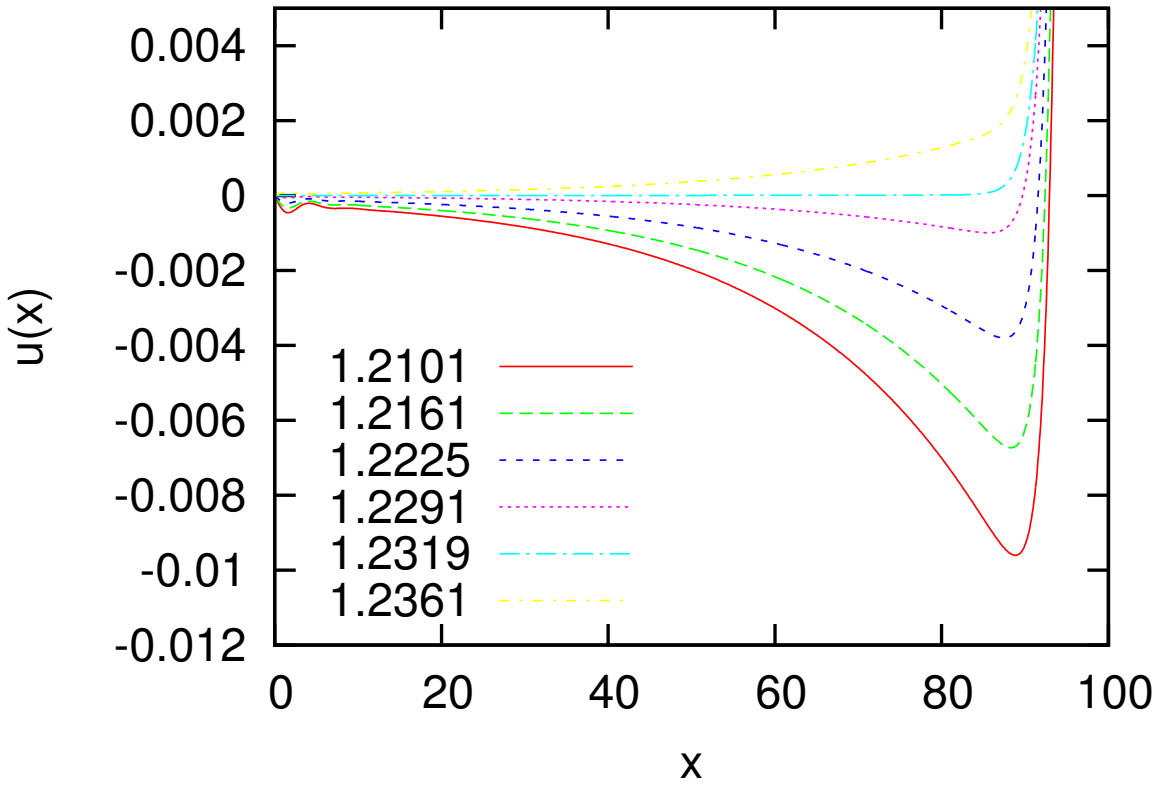

Figure 2.11: (Color online) A part of the profile of solutions obtained while the tracing (c) $\rightarrow$ (d) whose traveling velocity c is 1.2101(c), $1.2161, 1.2225, 1.2291, 1.2319$(d), 1.2361. The mechanism of this weakening of the localization is argued in Section 2.4.3.

In order to avoid the oscillation around the boundary, we focus on the tail of the solution. In Fig. 2.10, the oscillation seems to appear when the tail loses its flat part. Indeed, at $A_f = 0.2244$ where its flat part is around $[0, 60]$ and $A_f = 0.1254$ where it is around $[0, 40]$ the oscillation does not appear. We conclude that the disappearance of the flat part, which may occur when $A_f < 1.0$, is a precursor of the oscillation at the boundary. We call this decrease of the flat part "the weakening of the localization", and will discuss this mechanism in the next section.

We found that there exists a specific value c for each A_f such that the flat part recovers. Figure 2.11 shows the change in the tail of the solution while the continuation with c (A_f is fixed to 0.0496). At $c = 1.2319$ the flat part recovers to be $[0, 80]$. This continuation is the step (ii), and the "appropriate" value is $c = 1.2319$.

This "appropriate" value of c varies with A_f. In other words, the "appropriate" relation $c = c(A_f)$ defines a path on the two-dimensional parameter space c-A_f. Along this path the solution has always a flat part. In order to trace the solution along the path $c = c(A_f)$, however, it is necessary to express the condition $c = c(A_f)$ numerically. It can be easily done with the following integral value:

$$E_l = \int_0^l u(x)dx, \tag{2.7}$$

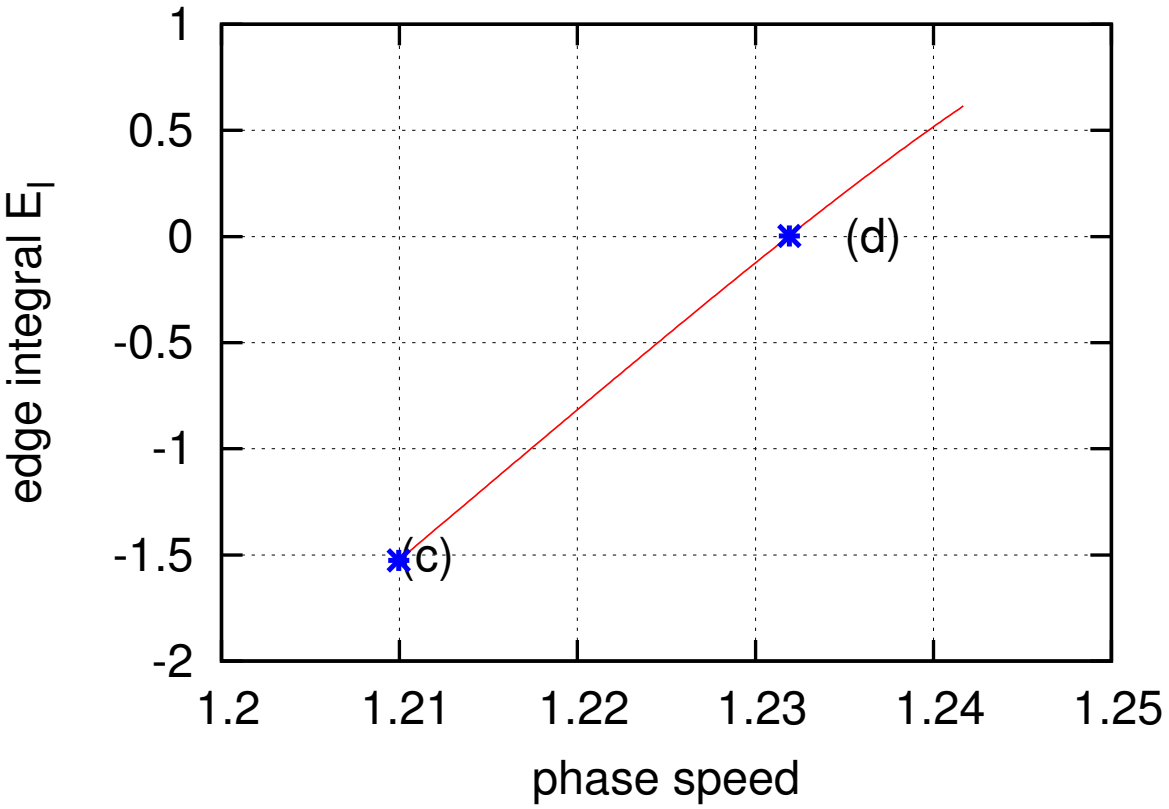

Figure 2.12: (Color online) E_l is plotted against the traveling velocity c. E_l measures how long the tail of the solution is. $E_l(c)$ cross the line $E_l = 0$, and this point is labeled (d). This crossing behavior is also argued in Section 2.4.3.

where l is chosen to be in the tail part. The change of E_l in the continuation mentioned above is shown in Fig. 2.12. The relation $c = c(A_f)$ is now implicitly defined by $E_l(c, A_f) = 0$. Then we can continuate the branch $u(x; c(A_f), A_f)$ with A_f. This conditional continuation can be implemented by a $(N+1)$-dimensional arc-length method, and we have succeeded to trace the solution till $A_f = 0$ within a numerical accuracy. This solutions is labeled as (e) in Fig. 2.8, and its profile is displayed in Fig. 2.13. Its propagation velocity $c_0 = c(0)$ equals to 1.2143. This is the same solitary-wave solution as that shown in fig.4c of [3].

2.4.3 Why the tail of the solution becomes longer?

In this subsection the mechanism of the weakening of the localization is considered. This weakening behavior enable us to obtain an implicitly defined path in A_f-c space. In order to generalize this technique to more complicated systems such as channel flows or pipe flows, it is necessary to investigate its details more precisely.

A steady localized solution $u(x)$ to Eq. (2.6) satisfies the ordinary differential equation:

$$\frac{d^4u}{dx^4} + \frac{d^2u}{dx^2} + (u - c)\frac{du}{dx} + A_f H(x)u = 0. \tag{2.8}$$

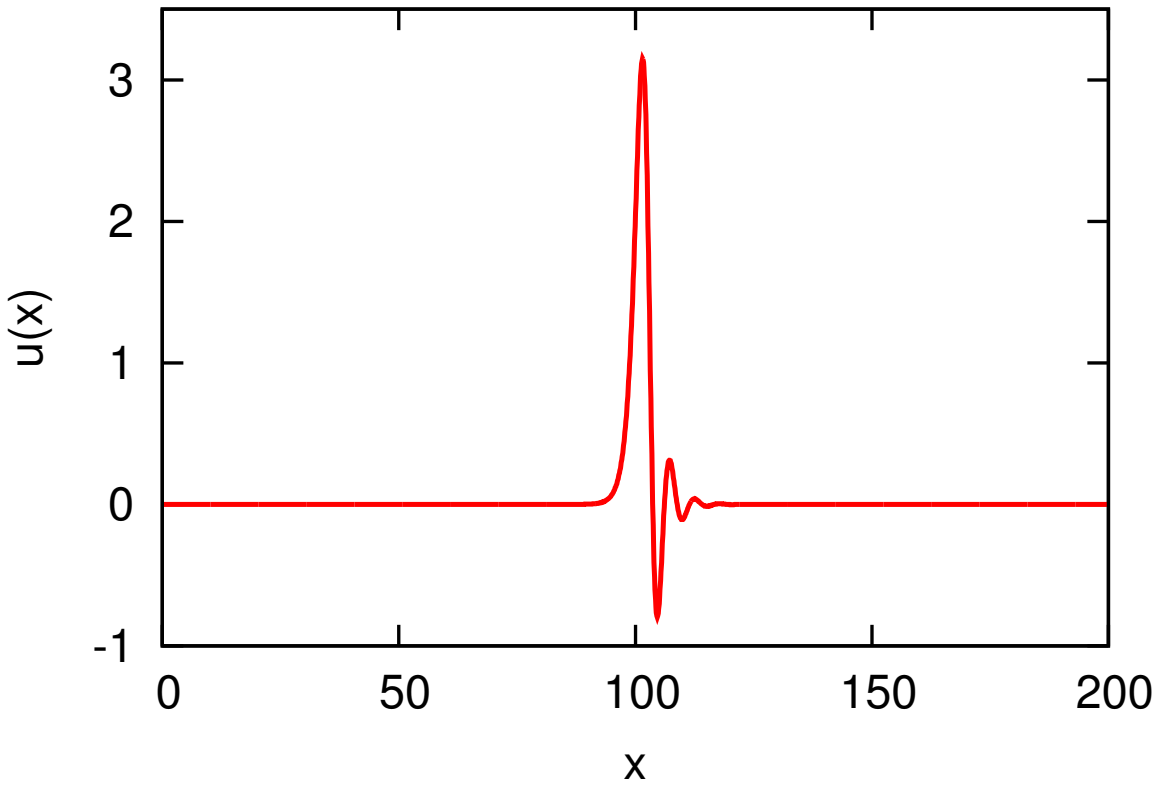

Figure 2.13: (Color online) The profiles of TWS to Eq. (2.5). It takes non-zero value on a region $[90 : 115]$, which is much wider than $\Omega = [97 : 103]$.

Here hats and primes are omitted for convenience. Regarding x as a virtual time, this equation defines a four-dimensional dynamical system. Then a localized solution $u(x)$ to Eq. (2.6) corresponds to a homoclinic orbit connecting the saddle point of this dynamical system, and the tails of the solution describes the asymptotic behavior of the homoclinic orbit from and to the saddle point. It should be noted that this reinterpretation has less compatibility with the fixed boundary condition $u(0) = u(L) = 0$ since we now consider the asymptotic behaviors in an infinite region $(-\infty, \infty)$ instead of the bounded region $[0, L]$. However the following arguments are all valid whenever $u(x)$ decays fast enough to be negligible comparing with the truncation error.

This dynamical system has a trivial fixed point (saddle point)

$$(u, \partial_x u, \partial_{xx} u, \partial_{xxx} u) = (0, 0, 0, 0)$$

corresponding to the solution $u(x) = 0$ to Eq. (2.6). The localized solution $u(x)$ can be regarded as a homoclinic trajectory of this trivial fixed point. Then the tail of the localized solution can be analyzed by the eigenvalues of Jacobi matrix of this dynamical system at the fixed point. Since $H(x)$ equals to 1 in the tail region, the eigen equation of the Jacobi matrix becomes as follows:

$$\lambda^4 + \lambda^2 - c\lambda + A_f = 0. \tag{2.9}$$

This quartic equation has two real roots λ_0, λ_1 and two complex roots $\lambda_\pm$. Since we focus on the case $A_f \ll 1$, we first consider the case $A_f = 0$, and then a perturbation expansion about A_f.

When $A_f = 0$, the eigenvalues are $\lambda_0 = 0$ and three roots of a cubic equation $\lambda^3 + \lambda - c = 0$. This cubic equation has a real root λ_1 and two complex roots

$$\lambda_\pm = (-\lambda_1 \pm i\sqrt{3\lambda_1^2 + 4})/2.$$

The real nonzero root λ_1 is positive when $c > 0$ and negative when $c < 0$, and here we consider the $c > 0$ case. Then the left and right tails of the solution can be written as follows:

$$u_L(x) = A_1 e^{\lambda_1 x}, \tag{2.10}$$

$$u_R(x) = A_+ e^{\lambda_+ x} + A_- e^{\lambda_- x}. \tag{2.11}$$

The coefficients A_1, A_+, A_- are determined in the nonlinear region. Since $\exp(\lambda_0 x)$ does not goes to zero as $x \to \pm\infty$,$u(x)$ cannot contain this term.

When $0 < A_f \ll 1$ the zero eigenvalue is modified as $\lambda_0 = A_f/c + O(A_f^2)$. Then the left tail of the solution can be written as follows:

$$u_L(x) = A_0 e^{\lambda_0 x} + A_1 e^{\lambda_1 x}. \tag{2.12}$$

The coefficients A_0 and A_1 are also determined in the nonlinear region, and depend both on c and A_f. Each of the terms in Eq. (2.12) defines a tail whose characteristic length is $1/\lambda_0$ and $1/\lambda_1$, and the realized tail is a superposition of them. As A_f goes to zero, the characteristic length $1/\lambda_0 = c/A_f$ diverges. Thus the modified eigenvalue λ_0 is the origin of the weakening, i.e., the long tail.

Next, we consider why we can obtain a solution with a short tail by the condition $E_l = 0$ for every small A_f. Using Eq. (2.12), E_l can be written as follows:

$$E_l \simeq \int_{-\infty}^{l} u_L(x)dx = \frac{A_0}{\lambda_0}e^{\lambda_0 l} + \frac{A_1}{\lambda_1}e^{\lambda_1 l}. \tag{2.13}$$

Since $1/\lambda_0 \gg 1/\lambda_1$ when $A_f \ll 1$, the first term in Eq. (2.12) is dominant except for a region near the nonlinear region. Thus the first term in Eq. (2.13) is rather dominant for an appropriate l. Then E_l roughly measures A_0, and $E_l = 0$ is realized when A_0 is zero where the tail by λ_0 disappears. A more precise argument is also possible. The condition $E_l = 0$ can yield the condition of A_0 as follows:

$$\begin{aligned} A_0 &= -\frac{\lambda_0}{\lambda_1}A_1 e^{(\lambda_1-\lambda_0)l} \\ &= -\frac{A_f}{c\lambda_1}A_1 e^{(\lambda_1-\lambda_0)l} + O(A_f^2). \end{aligned} \tag{2.14}$$

Thus A_0 is not exactly zero while $A_f > 0$. However, since λ_0 goes to zero as $A_f \to 0$, A_0 satisfying this condition also goes to zero.

The essence of the above arguments is the existence of the zero eigenvalue λ_0 and its modification due to the damping. The modified zero eigenvalue introduces another degree of freedom in the determination of tails of solutions. Calculating the eigenvector of the zero eigenvalue, it corresponds to a uniform level raising of the velocity field, $u(x) \mapsto u(x) + \delta c$, so it corresponds to Galilean invariance. In other words, the reason why this small eigenvalue appears is the breakdown of Galilean invariance. This fact indicates that such the weakening of the localization is expected to occur whenever a stream-wisely localized TWS is going to be obtained in Galilean-invariant systems by our method.

At last, we conclude this section with an error estimate. Since the continuous parameter dependence on c disappears when $A_f = 0$, the continuation becomes unstable as A_f goes to zero. Although the point $A_f = 0$ is a singular point in this continuation problem, A_f can get an arbitrary value as small as the numerical accuracy allows. Indeed, we get $A_f \sim 10^{-10}$ in the conditional continuation. This is as small as a threshold for Newton method, $\varepsilon_{\text{Newton}}$. Then the continuated solution can be regarded as a solution to KSE within an numerical error $\varepsilon_{\text{Newton}} + A_f\|u\|$.

2.5 Concluding Remarks

In this paper we introduce the damping filter method for obtaining spatially localized solutions. We adopt our method into two fundamental cases. First, in the Section 2.3, we consider localized solutions to Swift-Hohenberg equation (SHE). Then our method can not only reproduce known solutions, but also obtain another spatially localized solution which belongs to a closed isolated solution branch. Next, in the Section 2.4, we consider a stream-wisely localized traveling-wave solution (TWS) to Kuramoto-Sivashinsky equation (KSE). In this case, since the propagation velocity c is unknown, we have to continuate the solution with c and the filter amplitude A_f. In order to make continuation one-dimensional we introduce an implicit condition about the tail of solutions. Here we

reinterpret these result from a general point of view in order to adopt our method into more general cases.

The most interesting result in the Section 2.3 is the connection between two distinct solution branches. We show that two solution branches are connected with each other through the continuation with the filter amplitude A_f. We first introduce the filter term $-A_f H(x)u$ in order to obtain a guess at spatially localized solutions. However, it works as an excitation when $A_f < 0$. This excitation only works near the localized region where both $u(x)$ and $H(x)$ are non-zero. This causes an instability which may lead another localized solution. Indeed, we obtain the solution (d) in Section 2.3 only by the continuation with A_f. This spatially selective excitation mechanism has an advantage in searching spatially localized solutions. The result for SHE indicates that if another localized solution exists near the localized solution already obtained in the phase space, they may connect through this excitation mechanism. So our method may enable us to search localized solutions automatically.

In the Section 2.4, we have dealt with a spatially localized TWS to KSE. The main issue of this section is a treatment of the invariances. The damping filter term breaks the translational and Galilean invariances, but they recover when the filter disappears. This singular behavior is avoided by imposing the condition $c = c(A_f)$ by the implicit condition $E_l(c, A_f) = 0$.

This artificial condition can be reinterpreted as a critical line of the orbit-flip bifurcation [13]. For fixed A_f an orbit-flip bifurcation occurs when A_0, defined in Section 2.4.3, changes its sign with increasing c, see Fig. 2.9 and Fig. 2.11. Moreover, if $A_f \ll 1$, the relation $A_0 \sim A_f \sim 0$ holds on $c = c(A_f)$ because of Eq. (2.14). Therefore we can infer that the condition $c = c(A_f)$ corresponds to the critical line of the orbit-flip bifurcation in the four-dimensional ODE system Eq. (2.8).

To implement the critical condition directly, we can utilize an algorithm for tracking the orbit-flip bifurcation in AUTO [55]. This algorithm replaces the condition $E_l = 0$ with an orthogonal condition to keep the tangency between the homoclinic orbit and the leading eigenspace. Moreover, this method clarifies the mathematical meaning of our condition. However, since it is designed for a homoclinic orbit to ODE, it might be difficult to apply it for spatially two- or three-dimensional PDE systems. We thus expect that our method using E_l will be more suitable for the dynamical systems approach to turbulence.

Chapter 3

Ejection-Jet cycle: self-sustaining interface

3.1 Introduction

We focus on interfaces, which has critical importance to understand inhomogeneous systems since most properties changes along it. However, interfaces themselves can be complicated in strongly nonlinear inhomogeneous state. Turbulence-laminar interface appears most flows, e.g. boundary layers, jet, wake, and so on. In three dimensional flows, the dynamics of the interface is spatio-temporally chaotic [50]. It is sometimes even hard to detect the interface since they have intricate spatial geometry. These complexities prevent us from detail studies of interfaces. To avoid this problem, we use a two-dimensional channel flow, where interfaces become much quiet than those in three-dimensional flows. This will be one of the most simple example of localized chaotic coherent structures induced by spatial inhomogeneity.

This chapter consists of four sections. The Section 3.2 describes the simulation setting and shows an energy balance analysis. It is used to define a coherent structure, which we call chaotic interface. In Section 3.3, we confirm the self-sustainability of the chaotic interface using "filtered" simulations. Here we propose a self-sustaining mechanism of the chaotic interface, called ejection-jet cycle. A mechanism of determining the traveling speed of the interface is also argued. The last Section 3.4 give a short summary of this chapter.

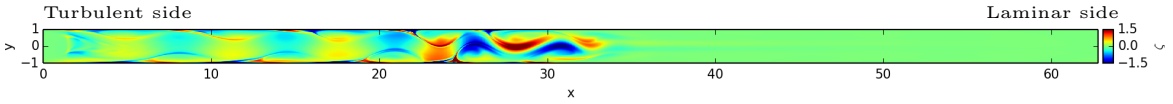

Figure 3.1: (color online) A snapshot of the vorticity deviation. ζ varies from -25 to 25 on the walls, and regions $\zeta > 1.5$ ($\zeta < -1.5$) are colored by the same color of $\zeta = 1.5$ ($\zeta = -1.5$).

3.2 chaotic interface structure

Two-dimensional laminar channel flow has the same critical Reynolds number Re_c as three-dimensional one. In 2D case, the TS-wave solution appearing at this critical point bifurcates into a weak chaotic state, which we call chaotic TS-wave, as its Reynolds number increases [4, 8, 9, 12]. In this paper, we consider a channel which contains both turbulent and laminar regions.

We adopt a frame of reference moving at a speed c_I against the laboratory frame for CI not to march, and call it interface frame. The streamwise and the wall-normal coordinates are denoted by x and y, respectively in this interface frame, and this system is non-dimensionalized by the half width of the channel, so that $y \in [-1, 1]$. The velocity field in this frame is denoted by $\boldsymbol{u}$. We deal with a very long box $[0, L = 20\pi] \times [-1, 1]$ to emulate the dynamics realized in an infinitely long channel. To clarify the direction we call the left side of Fig. 3.1 as the turbulent side, and the right side as the laminar side. Since the walls move in the interface frame, the non-slip boundary conditions become

$$\boldsymbol{u}(x, \pm 1) = -c_I \hat{\boldsymbol{x}},$$

where $\hat{\boldsymbol{x}}$ denotes the x directional unit vector. The Reynolds number Re is fixed to 8000 in this paper to exceed the critical value $Re_c = 5772$ of stability of the laminar flow. We have confirmed that the qualitative nature of CI reported below does not change for $Re = 6000$, 7000, 9000, and 10000.

To analyze the dynamics of this process in a finite computational box, we have to keep supplying laminar flow since the turbulent region becomes wider. We resolve this problem using the damping filter [52] in the interface frame. We introduce a linear damping term into the incompressible Navier-Stokes (NS) equation to reproduce a laminar Poiseuille flow

$$\boldsymbol{U}_L = (1 - y^2 - c_I)\hat{\boldsymbol{x}}$$

in a small region $\Omega = [0, 1.4] \times [-1, 1]$:

$$\frac{\partial \boldsymbol{u}}{\partial t} + (\boldsymbol{u} \cdot \nabla)\, \boldsymbol{u} = -\nabla p + \frac{1}{Re}\nabla^2 \boldsymbol{u} - H_{\sigma^2,\Omega}(x)\,(\boldsymbol{u} - \boldsymbol{U}_L)\,,$$
$$H_{\sigma^2,\Omega}(x) = \frac{1}{\sqrt{2\pi\sigma^2}} \int_\Omega dx' \exp\left(\frac{(x - x')^2}{2\sigma^2}\right),$$

where the last term of NS equation is the damping filter term. The periodic boundary condition is imposed in x-direction. Since c_I is larger than the phase velocity of the chaotic TS-wave, this damping term laminarizes it, and the laminarized flow returns upstream ($x = L$) due to the periodic boundary condition. We use the streamfunction-vorticity scheme, and thus the state variable is the z component of vorticity of the velocity deviation,

$$\zeta = (\nabla \times (\boldsymbol{u} - \boldsymbol{U}_L))_z\,.$$

We used Fourier(x)-Chebyshev(y) spectral method for spatial discretization, and explicit (convection term) and implicit (viscous term) Euler schemes for temporal evolution.

There were several steps to determine c_I. First, we created a uniform turbulent state in the laboratory frame using an initial condition

$$u(x, y, t = 0) = \varepsilon(1 - y^2)^2 \cos(kx)$$

like as [9], where $\varepsilon = 0.3$ and $k = 2\pi/L$. Second, we created a turbulent puff by executing short simulation in the laboratory frame with the damping filter $\Omega = [0, 20] \cup [40, L] \times [-1, 1]$. Third, we executed non-filtered simulation to estimate the c_I, This simulation suggests $c_I \simeq 0.8$. Last, we executed filtered simulation discussed above with $c_I = 0.8$. Then we adjusted c_I for the interface not to march, and this procedure yields $c_I = 0.855$.

In this setting a turbulent-laminar interface is simulated permanently. In Fig. 3.1, there are three regions: weak turbulence (WT, $x \lesssim x_l$), chaotic interface (CI, $x_l \lesssim x \lesssim x_r$), and laminar ($x_r \lesssim x$) regions. Moreover, the chaotic interface contains dynamic inner structures, a meandering bulk structure and strong wall shear layers. The weak turbulence consists of spatially modulated chaotic TS-waves [4].

To focus on its streamwise inhomogeneity, we consider the y-averaged energy balance equation:

$$\frac{\partial E}{\partial t} + \partial_x (J_u + J_\nu) = P_p + P_\nu - D_\nu + F. \tag{3.1}$$

The energy is defined in the interface frame:

$$E(x,t) = \int_{-1}^{1} dy \|\boldsymbol{u}\|^2/2.$$

Since the walls move, there is an energy injection due to the viscosity on the walls

$$P_\nu = P_\nu^+ + P_\nu^-,$$

where

$$P_\nu^\pm = \mp c_I \partial_y u_x|_{y=\pm 1}/Re$$

in addition to the bulk viscous dissipation

$$D_\nu = \frac{1}{Re} \int_{-1}^{1} dy \left(2 \left(\partial_x u_x \right)^2 + \left(\partial_x u_y \right)^2 + \left(\partial_y u_x \right)^2 \right). \tag{3.2}$$

The term

$$P_p(x,t) = -\int_{-1}^{1} dy \left(\boldsymbol{u} \cdot \nabla \right) p$$

denotes the energy injection due to the pressure gradient, and takes both positive and negative values. $P_p > 0$ means the flow accelerated by the pressure gradient, and $P_p < 0$ does the flow against the pressure gradient. P_p balances almost with the gradient of the energy flux $\partial_x J_u$, where

$$J_u = \int_{-1}^{1} dy u_x \|\boldsymbol{u}\|^2/2,$$

and their spatial means are smaller than those of the viscous terms P_ν and D_ν. The flux due to the viscosity J_ν is negligible.

$$F = -\int_{-1}^{1} dy H_{\sigma^2,\Omega} \boldsymbol{u} \cdot (\boldsymbol{u} - \boldsymbol{U}_L)$$

is the energy damping by the filter term.

To argue the energy balance of the chaotic interface, we give a definition of the separation points, x_l and x_r. We use the maximum point of the time-average of J_u, $x_l = 18.5$,

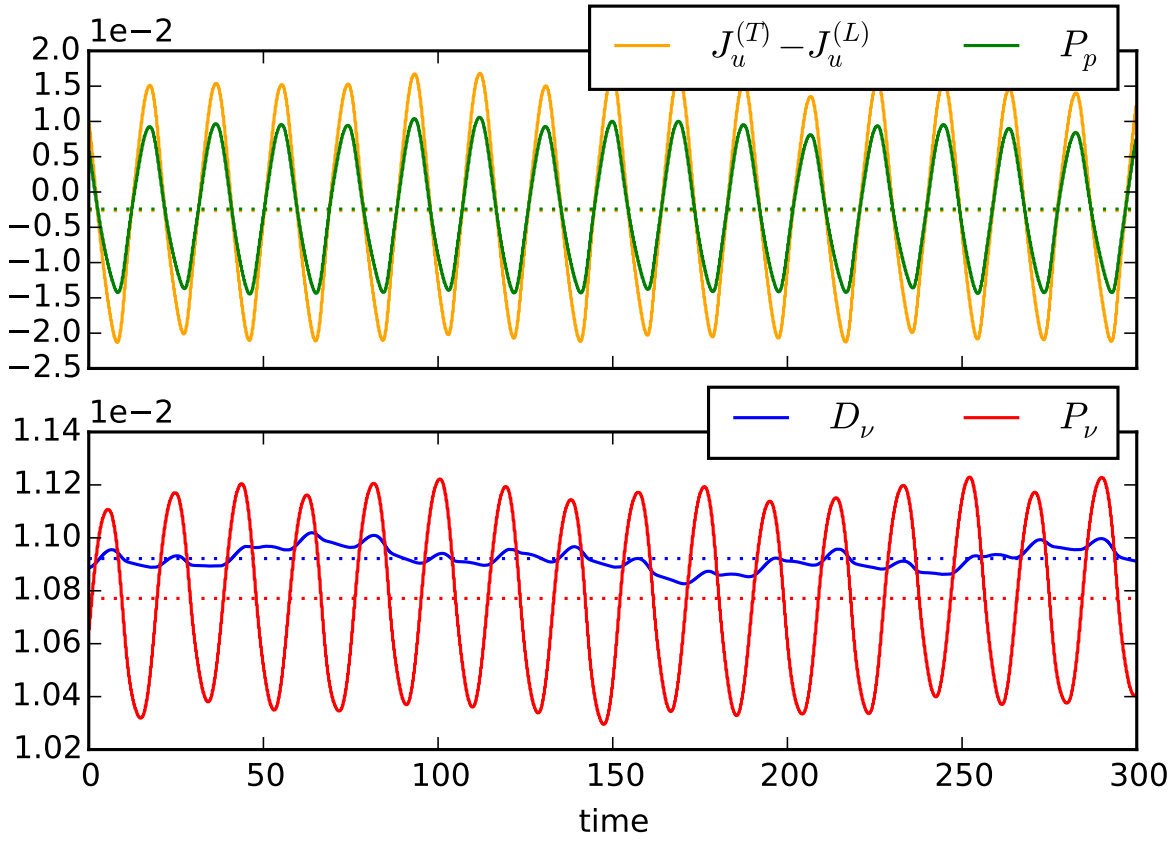

Figure 3.2: (color online) Time series of each integrated value in Eq. (3.3). They are weakly chaotic. Dotted lines of each color denote the mean values.

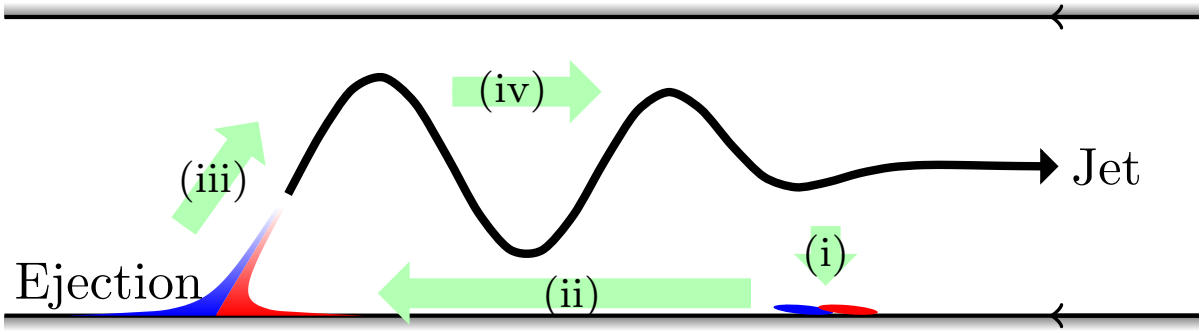

Figure 3.3: (color online) A schematic view of the ejection-jet cycle.

as the left side of CI. The right side $x_r = 35$ is determined by the decay of the wall vorticity. It will be well displayed in Fig. 3.5. Taking spatial integration of Eq. (3.1) over $[x_l, x_r]$, we obtain the following equation:

$$\frac{d\bar{E}}{dt} = J_u^{(L)} - J_u^{(T)} + \bar{P}_p + \bar{P}_\nu - \bar{D}_\nu, \tag{3.3}$$

where the bar $\bar{\cdot}$ denotes the integral over the interface, and $J_u^{(L)} = J_u(x_r), J_u^{(T)} = J_u(x_l)$ respectively. Since the interface marches faster than the mean flow, the energy flux of the laminar flow is negative in the interface frame. In other words, the chaotic interface withdraws the energy from the laminar flow by invading them. The time averages $\langle\cdot\rangle$ of these terms are calculated over $t \in [0, 300]$: $\left\langle J_u^{(L)} \right\rangle = -0.074$, $\left\langle J_u^{(T)} \right\rangle = -0.072$, $\left\langle \bar{P}_p \right\rangle = 2.4 \times 10^{-3}$, $\left\langle \bar{P}_\nu \right\rangle = 1.08 \times 10^{-2}$, $\left\langle \bar{D}_\nu \right\rangle = 1.09 \times 10^{-2}$, and the summation of them is almost zero: $\left\langle d\bar{E}/dt \right\rangle = 7.5 \times 10^{-5} \approx 0$. The time series of these values are displayed in Fig. 3.2. Each of these variables P_p, P_ν, and $J_u^{(T)} - J_u^{(L)}$ behave as chaotically amplified periodic motions. The periodicity strongly suggests the existence of a self-sustaining mechanism of the interface structure, and the chaotic amplitude suggests that its dynamics is effectively low-dimensional.

3.3 ejection-jet cycle

Here we give a concrete description of the self-sustaining mechanism of the chaotic interface. This sustaining process is constituted by the interaction among vortex ejections on the walls and the meandering jet in the bulk region. This collective dynamics is further split into four steps as summarized in Fig. 3.3. In the step (i), a pair of sheet-like vortices is created by the meandering jet. This process is taken place around $x \simeq x_r$ (see Fig. 3.5). In $x > x_r$ the jet becomes straight, and the creation of vortex pairs ceases.

The step (ii) is the convective growth of the vortex pair. The thin vortex pair generated in the step (i) grows up into an intense vortex ejection. To display this process, we use the intensity of the vorticity on the lower wall $\zeta_L(x,t) = \zeta(x, y = -1, t)$, which is displayed onto x-t plane in Fig. 3.4. Two dotted lines in this figure indicate that there are two traveling velocities except for c_I. The black dotted line guides the minimum of ζ_L around $x \in [20, 30]$ to measure the traveling velocity c_v of the vortex pair, and this line indicates $c_v \simeq 0.52$. Since we define the velocity in the laboratory frame, positive c_v

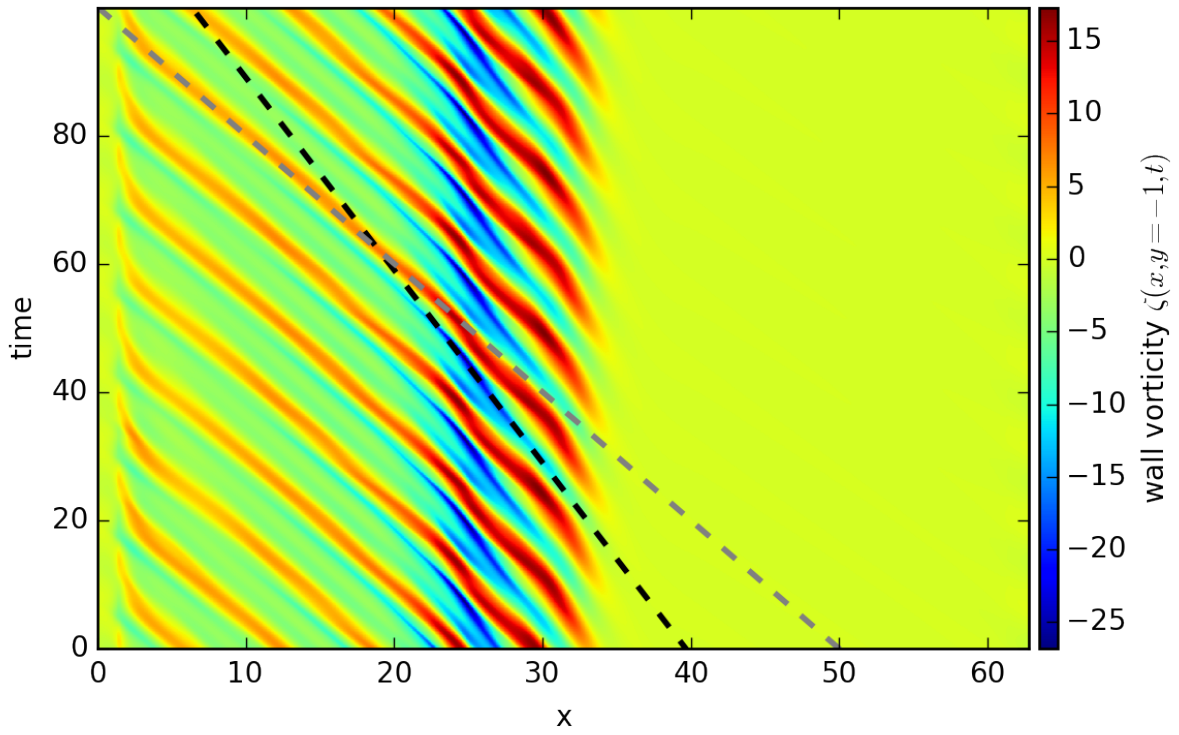

Figure 3.4: (color online) The vorticity at the lower wall $\zeta_L(x,t) = \zeta(x, y = -1, t)$. Black dotted line guides the minimum of $\zeta_L(x,t)$ (deep blue lines) around $x \in [20:30]$. The slope of this line indicates that local minimum points move as $x_{\min} = c_v' t \simeq -0.33t$, and thus they move with $c_v = c_I - c_v' \simeq 0.52$ in the laboratory frame.

means that the vortex pair goes to the laminar side in the laboratory frame, though it moves to the turbulent side in the interface frame since $c_v - c_I < 0$. The gray dotted line indicates the traveling velocity of weak turbulence $c_w = 0.38$, which is consistent with the previous work [4].

The step (iii) is the vortex ejection process, which excites the jet and makes it meander. This ejection occurs on the turbulent side of the chaotic interface, namely around $22 < x < 28$. A very strong shear accompanies this vortex ejection process. The wall unit l_τ is estimated at 2.1×10^{-3}, and the friction Reynolds number $Re_\tau = l_\tau^{-1}$ is about 460. This means that the width of the interface is 5000 times larger than l_τ. Therefore, we should regard this interface structure as a large-scale motion in the wall-turbulence context. After the intensive ejection process, the vortex structures are swept to turbulent side, and this corresponds to the leak of the energy $\langle \Delta J_u \rangle$ from the interface to the weak turbulence region.

The step (iv) is an energy transportation taken by the meandering jet. Most part of the fluid goes to the turbulent side in the interface frame since the invading speed $c_I = 0.855$ is faster than their traveling speeds, but the meandering jet goes to the laminar side even in the interface frame. The jet is strongly meandering around the ejection ($x \sim 25$) because of the alternate ejections on the lower and upper walls, and it becomes straight as leaving from the ejection. Then the cycle is closed, and we call this cycle an "ejection-jet" cycle (EJC).

To complete the EJC model, let us consider how the invading speed c_I is determined. There are two dynamical processes, the convective growth of the vortex pair and energy flux taken by the jet. The spatial growth of the vortex pair on the lower wall is displayed in Fig. 3.5. The maximum absolute value of the vorticity ζ is realized around $x = 25$, where the intensive ejection of the step (iii) occurs. The temporal minimum value of $\zeta(x, y = -1)$ changes linearly around $x \in [25, 35]$ as guided by a dotted line. Though the yielded graph is linear, it should be understood as an algebraic growth due to the nonlinear process of the step (ii). Since the vortex pair moves at the constant speed c_v in this region as shown in Fig. 3.4 (black dotted line), this spatial algebraic growth means a temporal algebraic growth of the minimum vorticity ω of the vortex pair in the Lagrangian viewpoint:

$$\omega = -\alpha(x - x_0) = \alpha(c_v - c_I)(t - t_0). \tag{3.4}$$

In addition, we assume the minimum of the vorticity $\omega_{\min} \approx -25$, which is realized around $x = 25$ on the lower wall, is independent of c_I. It should be determined only by Reynolds number. Then Eq. (3.4) gives a constant width of CI: $\Delta x = \omega_{\max}/\alpha$. The difference $c_I - c_v$ is regarded as the relative speed between the jet and the vortex pair, and thus it characterizes the mean shear exerting on the vortex pair. This means that the jet loses its energy for enhancing the vortex pairs. Here we can summarize the mechanism of the c_I determination. If c_I is too large, this energy loss prevents the creation of new vortex pairs, and thus c_I decreases. Conversely, if c_I is too small, the energy loss decreases, and thus the jet is accelerated. These two processes yield spontaneous determination of c_I. Quantitative validations of these assumptions are left for future works.

Let us review the EJC model by introducing filtered simulations. We make other three runs in which the filtered region Ω is set to damp one of the specific processes in the EJC, namely, (a) weak turbulence, (b) vortex ejection, and (c) vortex pair excitation.

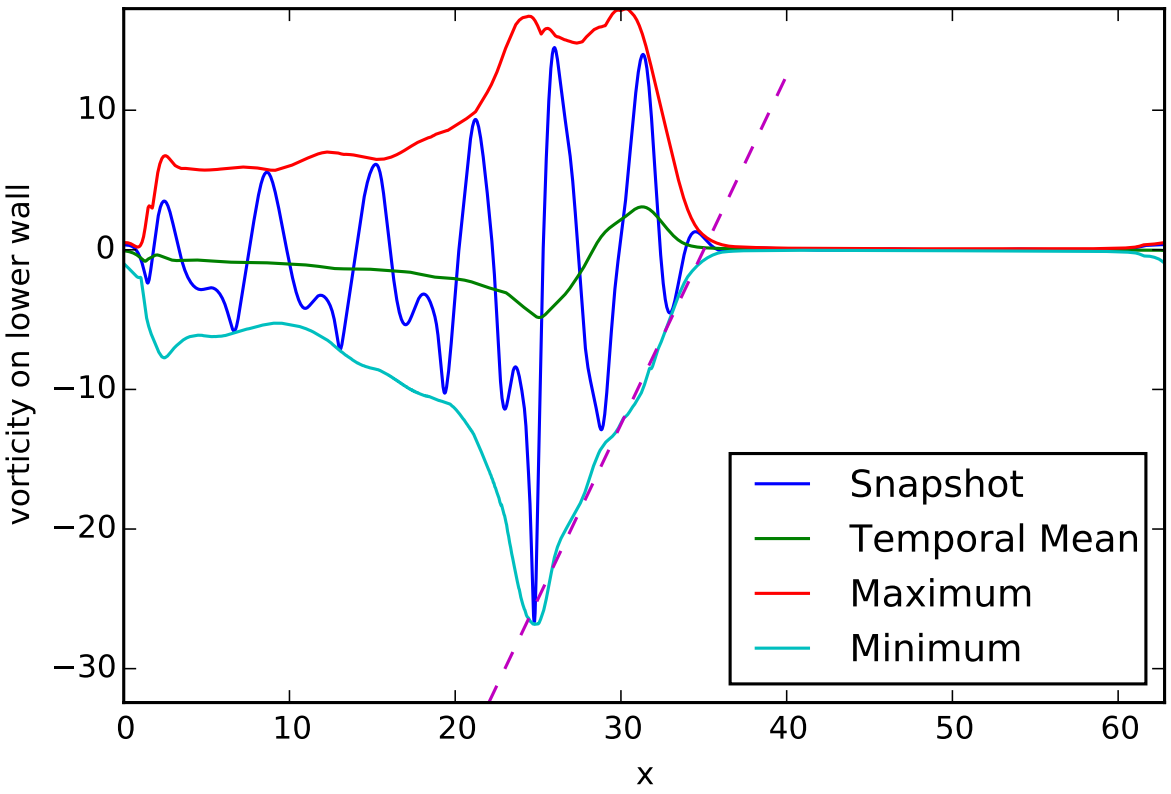

Figure 3.5: (color online) Spatial growth of the vorticity at the lower wall $\zeta_L(x,t) = \zeta(x, y = -1, t)$. A snapshot $\zeta_L(x, t = 58)$, temporal mean $\zeta_{\text{mean}}(x) = \langle \zeta_L(x,t) \rangle_t$, maximum $\zeta_{\text{max}}(x) = \max_{0 \le t \le T} \zeta_L(x,t)$, and minimum $\zeta_{\text{min}}(x) = \min_{0 \le t \le T} \zeta_L(x,t)$, are displayed with $T = 100$.

These filtered simulations help us confirm that these four steps are necessary and minimal components. A snapshot of the previous simulation is used as the initial condition of these filtered simulations. Animations visualized by the turbulent vorticity are included in the supplementary materials.

Case (a): we set $\Omega^{(a)} = [0, 22] \times [-1, 1]$ to damp the weak turbulent region, and to confirm the self-sustainability of the chaotic interface. In this setting we yield a permanent chaotic interface, whose invading speed and the spatial structure are hardly changed. We conclude that the following weak turbulence is additional as assumed in the EJC model. Furthermore, the selection process of c_I and the spatial structure is completely closed in the chaotic interface. In other words, the weak turbulence region hardly affects the selection process.

Case (b): we set $\Omega^{(b)} = [0, 30] \times [-1, 1]$ to confirm that the jet is maintained by the acceleration due to the vortex ejection. If the meandering jet is self-sustaining, this simulation could yield a permanent finite amplitude solution. However, the laminar flow has occupied whole region. In this sense, the meandering of the jet is only a component mechanism of this self-sustaining process, and is not self-sustaining.

Case (c): we set $\Omega^{(c)} = [30, 20\pi] \times [-1, 1]$ to obstruct the step (i). In this case the non-filtered region of the chaotic interface ($20 < x < 30$) keeps alive on the same position until $t \lesssim 20$, and then it travels to the turbulent side. This time lag corresponds to the growth time T_v of the vortex ejection, and thus this result also supports the EJC model. After a long transient, another chaotic interface is reconstructed around $15 \lesssim x \lesssim 27$. Their invading speed and spatial structure are same as the previous one. This result insists that the chaotic interface structure is robust while a laminar region exists. This robustness is an important issue for the pattern selection problem, but the current framework of the dynamical systems approach lacks tools applicable for settling this issue.

3.4 Concluding Remarks

We have investigated the turbulent-laminar interface in two-dimensional channel flow, and proposed a novel self-sustaining mechanism, ejection-jet cycle (EJC). In a technical viewpoint, the filtered simulation has been introduced, and utilized to confirm the self-sustainability of EJC.

Comparing from simple interfaces like shocks in compressible fluids, the chaotic interface (CI) has internal dynamics. It is hard to capture such dynamical properties in current approaches to interfaces. For example, there is a classical heteroclinic orbit technique [19], which has been developed to analyze effectively one-dimensional interfaces. This method rephrases the spatial structure of the interface into a heteroclinic orbit of a corresponding low-dimensional dynamical system, and thus it is incompatible to time-dependent interface. Our approach to treat the local self-sustainability directly by the filtered simulations will be an alternative approach to attack dynamical interfaces. It is well compatible with the coherent structure approach since the interface itself would be a coherent structure.

Chapter 4

General Conclusion

4.1 Damping filter method

In chapter Chapter 2, we have introduced the damping filter method for obtaining spatially localized solutions. The damping term works on a filtered region Ω, and vanishes out of Ω (unfiltered region). An exact solution of this filtered equation is connected to a solution of original equation by executing a continuation. The damping filter term enables us to extract local dynamics as a localized solution. This method has been applied to Swift-Hohenberg equation and Kuramoto-Sivashinsky equation. Technical issues in the continuation process have been successfully resolved.

Since localized exact solutions provide abundant information about local dynamics, we intend to apply this filtering method for mature turbulence in which the techniques used in weak turbulence to obtain localized solutions may not expect to work well. Moreover, different from approximate techniques, e.g. proper orthogonal decomposition [7] and Koopman mode decomposition [21], the exact solutions allow us to analyze their stabilities and origins using bifurcation diagrams. Such global information helps us understand when and why the local dynamics appears and even how to control it. It should be noted that such localized exact solutions sometimes do not exist in mature turbulence because of the properties of its local dynamics. Even for these cases, however, the filtered simulations can be of advantage to seeking localized dynamics embedded in mature turbulence as shown in Chapter 3.

4.2 Ejection-Jet cycle

We have investigated the novel self-sustaining mechanism, we call ejection-jet cycle (EJC). EJC is realized in two-dimensional channel flows at relatively high Reynolds number $Re = 6000$ to 10000. This self-sustaining mechanism describes a synchronized interscale collective dynamics: This cycle consists of the meandering jet corresponding to outer-wall dynamics of the outer scale and the vortex pairs corresponding to the inner-wall dynamics of the wall scale. While Waleffe's self-sustaining process [11] utilizes an absolute instability, the EJC model does a convective instability, which needs sufficient space to grow up. That is, the convective instability makes it possible for the structures of the two different scales to interact with each other. This two-scale interaction mechanism may

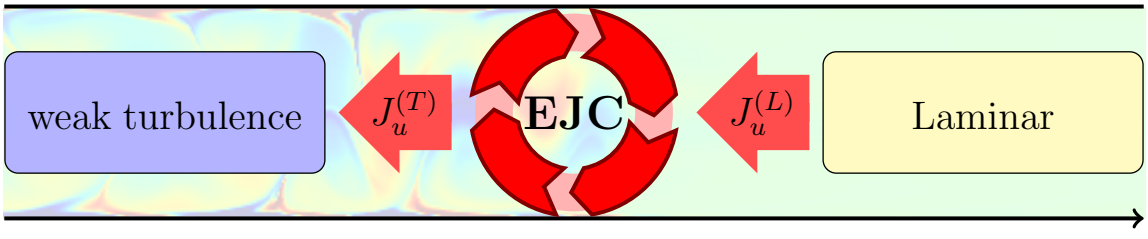

Figure 4.1: The chaotic interface (CI) as a functional coherent structure (FCS). CI pumps energy from the laminar part ($J_u^{(L)}$) to the following weak turbulent region ($J_u^{(T)}$).

be applied for the large-scale motion in three-dimensional wall-turbulence [22], although the chaotic nature of CI is far weaker than that of three-dimensional wall-turbulence. We should try to combine such a convective interaction scenario with the wall-turbulence theories, namely the mixing length picture and/or the attached eddy picture, and this remains as our future works.

In the damping filter method argued in Chapter 2, the damping filter is finally removed. However, we cannot obtain an exact localized solution to Navier-Stokes equation corresponding to CI because CI have to feed the weak turbulence region. This additional "role" uncloses the self-sustaining dynamics of CI. Spatially-localized coherent structures can be represented by localized exact solutions to exact, i.e. unfiltered Navier-Stokes equation if they are governed by closed dynamics. We call them "isolable" coherent structures, and have shown that EJC is locally self-sustaining but is not isolable. We rather expect that such unclosed local self-sustaining dynamics is ubiquitous in developed and mature turbulences where hypothetical coherent structures, i.e., vortices play a role in energy or momentum cascades in scale or physical spaces. Therefore, the filtered simulation is expected to be available to isolate such unclosed dynamics.

4.3 Functional Coherent Structures

Two-dimensional channel is one of simple examples where the local dynamics is not isolated. EJC robs energy from the laminar flow, and gives some energy to the following weak turbulence region (WT). The filtered simulations reveal the self-sustainability of the chaotic interface (CI) and its minimal mechanism, i.e. ejection-jet cycle. The chaotic interface should be regarded as a spatially-localized coherent structure, and thus this system can be understood in the dynamical systems viewpoint. However, strictly speaking the dynamics of CI is not isolated and significantly different properties from localized coherent structures discussed in the exact solution based dynamical systems approach. Rather, these properties are significantly similar to the fundamental processes of Richardson's energy cascade and the log layer as we discussed on mature turbulence in the introduction. Two different type of coherent structures, i.e. CI and WT are spatially segregated, and they make up the one-sided interaction. Thus, this system is categorized in mature turbulence.

We introduce "functional" coherent structure (FCS) to denote the chaotic interface (CI). Since CI has the "role" in addition to the unclosed dynamics as noted above and the role represents some "function", we adopt these properties as the definition of FCS.

In general, we use a functional coherent structure to describe a locally self-sustaining coherent structure of which local dynamics is unclosed due to its additional function. In this sense, the FCS-based dynamical systems approach can be called role-based approach. FCS is characterized by its additional role: The role of CI is to pump energy from the laminar flow to the following weak turbulence region.

While the turbulence-laminar interface in two-dimensional channel flow is a single FCS system, we can consider multiple FCS systems where FCSs work cooperatively, and we expect that the Richardson's cascade is one of them. Although the original cascade picture is discussed in the scale (wave-number) space, recent studies try to detect its fundamental process as a spatially localized dynamics. To realize this attempt, we have to solve several technical and theoretical issues. One large problem is the creation and annihilation of FCS. The vortex structures corresponding to the fundamental process of Richardson's cascade seem not to be persistent. Such a coherent structure repeats creation, annihilation and even swept away. We expect that these fragile FCS could be represented with some Lagrangian picture and local saddle-like phase space structure. These expectations will be confirmed in our future works.

Bibliography

[1]D. Coles, "Transition in circular Couette flow", Journal of Fluid Mechanics **21**, 385–425 (1965).

[2]B. Cantwell, D. Coles, and P. Dimotakis, "Structure and entrainment in the plane of symmetry of a turbulent spot", Journal of Fluid Mechanics **87**, 641–672 (1978).

[3]D. Michelson, "Steady solutions of the Kuramoto-Sivashinsky equation", Physica D: Nonlinear Phenomena **19**, 89–111 (1986).

[4]J. Jiménez, *Transition to turbulence in two-dimensional Poiseuille flow*, 1990.

[5]M. Nagata, "Three-dimensional finite-amplitude solutions in plane Couette flow: bifurcation from infinity", Journal of Fluid Mechanics **217**, 519–527 (1990).

[6]J. Jimeez and P. Moin, "The minimal flow unit in near-wall turbulence", Journal of Fluid Mechanics **225**, 213–240 (1991).

[7]G. Berkooz, P. Holmes, and J. Lumley, "The proper orthogonal decomposition in the analysis of turbulent flows", Annual Review of Fluid Mechanics **25** (1993).

[8]A Fortin, M Jardak, J. Gervais, and R Pierre, "Old and new results on the two-dimensional Poiseuille flow", Journal of Computational Physics **115**, 455–469 (1994).

[9]M. Umeki, *Numerical simulation of plane Poiseuille turbulence*, 1994.

[10]U. Frisch, *Turbulence: the legacy of AN Kolmogorov* (Cambridge university press, 1995).

[11]J. M. Hamilton, J. Kim, and F. Waleffe, *Regeneration mechanisms of near-wall turbulence structures*, 1995.

[12]a. Rauh, T. Zachrau, and J. Zoller, *Nonlinear stability analysis of plane poiseuille flow by normal forms*, 1995.

[13]A. Champneys, Y. A. Kuznetsov, and B. Sandstede, "A NUMERICAL TOOLBOX FOR HOMOCLINIC BIFURCATION ANALYSIS", International Journal of Bifurcation and Chaos **06**, 867–887 (1996).

[14]F. Waleffe, "On a self-sustaining process in shear flows", Physics of Fluids **9**, 883–900 (1997).

[15]S. Balbus and J. Hawley, "Instability, turbulence, and enhanced transport in accretion disks", Reviews of Modern Physics **70**, 1–53 (1998).

[16]J. Jiménez and M. P. Simens, "Low-dimensional dynamics of a turbulent wall flow", Journal of Fluid Mechanics **435**, 81–91 (2001).

[17]G. Kawahara and S. Kida, "Periodic motion embedded in plane Couette turbulence: regeneration cycle and burst", Journal of Fluid Mechanics **449**, 291–300 (2001).

[18]Y. Kuramoto, *Chemical oscillations, waves, and turbulence* (Courier Corporation, 2003).

[19]W. van Saarloos, "Front propagation into unstable states", Physics Reports **386**, 29–222 (2003).

[20]D. M. Abrams and S. H. Strogatz, "Chimera States for Coupled Oscillators", Physical Review Letters **93**, 174102 (2004).

[21]I. Mezić and S. Barbara, "Spectral Properties of Dynamical Systems, Model Reduction and Decompositions", Nonlinear Dynamics **41**, 309–325 (2005).

[22]S. TOH and T. ITANO, *Interaction between a large-scale structure and near-wall structures in channel flow*, 2005.

[23]B. Hof, J. Westerweel, T. M. Schneider, and B. Eckhardt, "Finite lifetime of turbulence in shear flows.", Nature **443**, 59–62 (2006).

[24]J. Burke and E. Knobloch, "Homoclinic snaking: structure and stability.", Chaos **17**, 037102 (2007).

[25]Kazumasa Takeuchi, Masafumi Kuroda, Hugues Chaté, and Masaki Sano, "Directed Percolation Criticality in Turbulent Liquid Crystals", Physical Review Letters **99** (2007) 10.1103/PhysRevLett.99.234503.

[26]T. M. Schneider, B. Eckhardt, and J. A. Yorke, "Turbulence Transition and the Edge of Chaos in Pipe Flow", Physical Review Letters **99** (2007) 10.1103/PhysRevLett.99.034502.

[27]A. Bergeon and E. Knobloch, "Spatially localized states in natural doubly diffusive convection", Physics of Fluids **20**, 034102 (2008).

[28]R. Goto, S. Fujiyama, H. Yano, Y. Nago, N. Hashimoto, K. Obara, O. Ishikawa, M. Tsubota, and T. Hata, "Turbulence in Boundary Flow of Superfluid He4 Triggered by Free Vortex Rings", Physical Review Letters **100**, 045301 (2008).

[29]E. Knobloch, "Spatially localized structures in dissipative systems: open problems", Nonlinearity **21**, T45–T60 (2008).

[30]M. Beck, J. Knobloch, D. J. B. Lloyd, B. Sandstede, and T. Wagenknecht, "Snakes, Ladders, and Isolas of Localized Patterns", SIAM Journal on Mathematical Analysis **41**, 936–972 (2009).

[31]Y. Duguet, P. Schlatter, and D. S. Henningson, "Localized edge states in plane Couette flow", Physics of Fluids **21**, 111701 (2009).

[32]T. Ishihara, T. Gotoh, and Y. Kaneda, "Study of High – Reynolds Number Isotropic Turbulence by Direct Numerical Simulation", Annual Review of Fluid Mechanics **41**, 165–180 (2009).

[33]T. Schneider, D. Marinc, and B. Eckhardt, "Localised edge states nucleate turbulence in extended plane Couette cells", Journal of Fluid Mechanics **646**, 15 (2009).

[34]Y. Duguet, P. Schlatter, and D. S. Henningson, "Formation of turbulent patterns near the onset of transition in plane Couette flow", Journal of Fluid Mechanics **650**, 119–129 (2010).

[35]T. M. Schneider, J. F. Gibson, and J. Burke, "Snakes and Ladders: Localized Solutions of Plane Couette Flow", Physical Review Letters **104**, 104501 (2010).

[36]K. Avila, D. Moxey, A. de Lozar, M. Avila, D. Barkley, and B. Hof, "The onset of turbulence in pipe flow.", Science (New York, N.Y.) **333**, 192–6 (2011).

[37]D. Barkley, "Simplifying the complexity of pipe flow", Physical Review E - Statistical, Nonlinear, and Soft Matter Physics **84**, 016309 (2011).

[38]G. Kawahara, M. Uhlmann, and L. van Veen, "The Significance of Simple Invariant Solutions in Turbulent Flows", Annual Review of Fluid Mechanics **44**, 203–225 (2011).

[39]J. Knobloch, D. J. B. Lloyd, B. Sandstede, and T. Wagenknecht, "Isolas of 2-Pulse Solutions in Homoclinic Snaking Scenarios", Journal of Dynamics and Differential Equations **23**, 93–114 (2011).

[40]M. Sipos and N. Goldenfeld, "Directed percolation describes lifetime and growth of turbulent puffs and slugs", Physical Review E **84**, 035304 (2011).

[41]K. T. Allhoff and B. Eckhardt, "Directed percolation model for turbulence transition in shear flows", Fluid Dynamics Research **44**, 031201 (2012).

[42]S. Goto, "Coherent Structures and Energy Cascade in Homogeneous Turbulence", Progress of Theoretical Physics Supplement **195**, 139–156 (2012).

[43]P. Manneville, "Turbulent patterns in wall-bounded flows: A Turing instability?", EPL (Europhysics Letters) **98**, 64001 (2012).

[44]M. Avila, F. Mellibovsky, N. Roland, and B. Hof, "Streamwise-localized solutions at the onset of turbulence in pipe flow", Physical Review Letters **110**, 224502 (2013).

[45]A. Haimovici, E. Tagliazucchi, P. Balenzuela, and D. R. Chialvo, "Brain Organization into Resting State Networks Emerges at Criticality on a Model of the Human Connectome", Physical Review Letters **110**, 178101 (2013).

[46]T. Ishihara, Y. Kaneda, and J. C. R. Hunt, "Thin Shear Layers in High Reynolds Number Turbulence—DNS Results", Flow, Turbulence and Combustion **91**, 895–929 (2013).

[47]Kengo Deguchi, Philip Hall, and Andrew Walton, "The emergence of localized vortex – wave interaction states in plane Couette flow", Journal of Fluid Mechanics **721**, 58–85 (2013).

[48]J. J. Arenzon, A. Coniglio, A. Fierro, and M. Sellitto, "Percolation approach to glassy dynamics with continuously broken ergodicity", Physical Review E **90**, 020301 (2014).

[49]K Deguchi and P Hall, "Canonical exact coherent structures embedded in high Reynolds number flows", Philosophical Transactions of the Royal Society A: Mathematical, Physical and Engineering Sciences **372**, 20130352–20130352 (2014).

[50]T. Ishihara, H. Ogasawara, and J. C. Hunt, "Analysis of conditional statistics obtained near the turbulent/non-turbulent interface of turbulent boundary layers", J. Fluid Struct. **53**, 50–57 (2014).

[51]T. Kreilos, B. Eckhardt, and T. M. Schneider, "Increasing Lifetimes and the Growing Saddles of Shear Flow Turbulence", Physical Review Letters **112**, 044503 (2014).

[52]T. Teramura and S. Toh, "Damping filter method for obtaining spatially localized solutions", Physical Review E - Statistical, Nonlinear, and Soft Matter Physics **89**, 052910 (2014).

[53]R. Venugopalan, "Thermalization of the world's smallest fluids: Recent developments", Nuclear Physics A **928**, 209–221 (2014).

[54]T. Yasuda, S. Goto, and G. Kawahara, "Quasi-cyclic evolution of turbulence driven by a steady force in a periodic cube", Fluid Dynamics Research **46**, 061413 (2014).

[55]E. J. Doedel, R. C. Paffenroth, A. R. Champneys, T. F. Fairgrieve, Y. A. Kuznetsov, B. E. Oldeman, B Sandstede, and X. J. Wang, "AUTO-07P: Continuation and bifurcation software for ordinary differential equations (2007)", http://indy.cs.concordia.ca/auto/.